NTNU – Trondheim
Norwegian University of
Science and Technology

STRUCTURE OF PARAFFIN WAX DEPOSITS IN SUBSEA PIPELINES

Margaret Kjøraas

Petroleum Geoscience and Engineering
Submission date: June 2013
Supervisor: Jon Steinar Gudmundsson, IPT

Norwegian University of Science and Technology
Department of Petroleum Engineering and Applied Geophysics

Abstract

This master thesis tries to investigate the effects of rough surfaces. The analysis is done by use of ANSYS Technology Inc's Software FLUENT, where three different geometries are simulated in order to achieve the resulting friction factor. To compare and analyze the obtained results, methods to calculate the friction factor presented in previous published literature is included. The results obtained in this report are subject to uncertainties related to simulation inexperience, and the possible misinterpretation of one of the methods presented.

The results confirms that rippled deposits yields higher friction factors than rectangular deposits, and that rectangular leads to higher results for the friction factor than sand grain roughness. There are, however, deviations between some simulations and their corresponding calculated values which is unexpected.

Eventhough the origin of this report is to shed some light on the structure of wax deposits, the focus lies more on general roughness structures and the investigation of these. It remains for future work to link results to a given wax deposition situation.

Sammendrag

Utgangspunktet for denne masteroppgaven er ønsket om å avdekke effekter relatert til ulike ruhetsmiljøer, i lys av å utforske hvilke konsekvenser dette kan ha for et rør med voksavsetning. Dette har hovedsaklig blitt gjort gjennom simuleringer i ANSYS Technologys programvare FLUENT. Tre ulike ruhetsmiljøer har blitt simulert i forbindelse med denne oppgaven. For å kunne evaluere oppnådde resultater, har det blitt utført en sammenligning opp mot utregnede verdier fra et par metoder funnet i tidligere utgitt litteratur. Det følger usikkerheter med resultatene i denne oppgaven, dette pågrunn av lite erfaring med FLUENT. Det er også mulig at mistolkning av metodene presentert i litteraturen er en mulig feilkilde.

Effekten på friksjonsfaktoren er størst for ruhet dannet av rifler, videre er effekten også større for rektangulær ruhet sammenlignet med sandkornruhet.

Selv om utgangspunktet for denne oppgaven stammer fra voksproblematikk i rør, så har fokuset vært å utforske ulike ruhetstrukturer og effektene av disse. Det gjenstår å knytte disse resultatene opp mot en voksavsetning-situasjon for eventuelle oppgaver i fremtiden.

Preface

This thesis was written in the spring semester 2013 and presents my work in TPG4905 Petroleum Technology at The Norwegian University of Science and Technology (NTNU).

The master thesis has been written under the supervision of Jon Steinar Gudmundsson. I would first and foremost, thank him for hours spend guiding and helping me acquire more knowledge on the area of wax deposition and roughness.

As the master thesis is the final work in connection with my degree, Master in Petroleum Production at NTNU, I would like to thank teachers I have had during these past five years. Also, friends and family that has contributed with support and enjoyment are very much appreciated!

Being motivated and happy during this process has been very important. Besides acquiring interesting knowledge, a lot of my motivation has come from spending time with friends, often in combination with physical training such as climbing and mountain hikes. An amazing trip to Malaysia, as a part of the main excursion 2013, was also extremely appreciated. Thank you all for wonderful memories that will last for life!

I hereby certify that this work is exclusively my own.

Contents

List of Tables

List of Figures

Symbols

Ch. 3	Name	Unit
n	Mass Flux	kg/sm^2
ρ	Density	kg/m^3
D	Diffusion Constant	m^2/s
$\frac{dC}{dr}$	Concentration Gradient	$1/m$
$\frac{dC}{dT}$	CG to Temperature	$1/°C$
$\frac{dT}{dr}$	Temperature Gradient	$°C/m$
$\frac{dx}{dt}$	Deposition Gradient	m/s
x_D	Deposition Rate	kg/s
x_R	Rate of Removal	kg/s
k_1	Empirical Constant	-
k_2	Empirical Constant	-
ΔP	Pressure Drop	Pa
P	Pressure	Pa
f_D	Darcy Friction Factor	-
L	Length	m
d	Diameter	m
r	Radius	m
u	Velocity	m/s
q	Flow Rate	m^3/s
π	PI	-
μ	Dynamic Viscosity	Pas
ϕ_i^{0L}	Liquid Phase Fugacity	-

Ch. 3	Continued	
x_i^S	Phase Mole Fraction	-
f_i^S	Fugacity	Pa
T	Temperature	K
T_i^f	Melting Temperature	K
R	Universal Gas Constant	$J/Kmol$
ΔH_i^f	Enthalpy of Fusion	J/g
Ch. 4		
λ	Friction Factor	-
G	Geometry Factor	-
R	Roughness Function	-
R_0	Fictious RF	-
R_{k_1,k_2}	Fitted RF	-
R_{0k_1,k_2}	Fictious Fitted RF	-
a_1	Constant	-
a_2	Constant	-
a_3	Constant	-
a_4	Constant	-
p	Pitch	m
w	Width	m
h	Height	m
h^+	Dimensionless Height	-
u^*	Friction Velocity	m/s

Ch. 4	**Continued**	
ν	Kinematic Viscosity	m^2/s
z_k	Relationship of h/L	-
B	Roughness Function	-
k	Roughness Height	-
k^+	Dimensionless RH	-
u_τ	Shear Velocity	m/s
A	Asymptotic Level	m
b	Time Variable	s^{-1}
A_E	Edmonds AL	m
B	Edmonds Decay Constant	m
C	Edmonds Time Variable	s^{-1}
St_s	Stanton Number	-
f_s	Smooth Friction Factor	-
Pr	Prandtl Number	-
Re	Reynolds Number	-
e^+	Dimensionless RH	-

Ch. 5		
k	Turbulent Kinetic Energy	m^2/s^2
ϵ	Turbulent Dissipation Rate	m^2/s^2
k_s	FLUENT RH	m
C_s	FLUENT RC	-
Ch. 7		
ΔB	FLUENT RF	-
κ	Van Karmen Constant	-
k_s^+	FLUENT Dimensionless RH	-

1. Introduction

In recent years, the production of offshore oil and gas reservoirs has shifted towards being transported through long subsea pipelines. Harsher environment, and lack of transport infrastructure available makes transport of hydrocarbons in subsea pipelines an attractive solution. However, this is not a flawless solution as problems such as hydrate slugging, asphaltenes and wax deposition can imply restrictions to the flow. Among these, wax deposition on the pipeline surface has become the most significant problem in later years (Huang 2011).

Wax deposition in a pipeline occurs when crude oil or a condensate experience reduced temperature due to cooling by the surrounding seawater. Typical reservoir temperatures are found between 70°C - 150°C (Huang 2011). At these temperatures the wax forming components are in solution, and will behave as a normal oil or condensate. As soon as the temperature drops below a certain temperature, usually referred to as the Wax Appearance Temperature (WAT) or the cloud point, wax starts to precipitate out of the oil. The precipitated wax crystalizes and become solid material, either flowing in the oil, or entrapped in a layer sticking to the pipe wall. The size and shape of the deposited layer is difficult to precisely model. While extensive research have given great insight to the matter, many areas of this problem remains unanswered.

The aim of this thesis is to investigate the roughness belonging to the wax layer. Previous knowledge shows that roughness change the heat transfer across a given boundary layer, which will affect the deposition trend. Heat transfer is not the topic of this thesis, and it is therefore left for future works to investigate this. Attempts to

simulate possible roughness effects in ANSYS Technology Inc's software FLUENT will be the focus of most of this report. The simulations will investigate what effects different geometries might have on the resulting pressure drop. The results will be compared to calculated friction factors, resulting from different models presented in the literature.

The thesis will also take a look into some existing models for predicting wax deposition, though more or less all of these models do not incorporate any effects of roughness.

2. Characteristics of a Wax Layer

Wax that deposits at the interference of a subsea pipeline will in most cases be removed from the surface by routine pigging. The pigging results in deformed or ruined samples of wax entering the surface for inspection. As a result, visual inspection becomes difficult. In order to establish the layer's correct thickness or inherent roughness, other more theoretical methods needs to be used.

One reason for wanting knowledge on the roughness is that several research papers have reported that an overestimation of wax layers often occur. By use of an analysis of the induced pressure drop a thickness of the wax layer may be derived by comparing it to a pipe with no wax present. It is known that a rough surface will increase the pressure drop in a turbulent regime, thus a higher pressure drop will not necessarily mean a thicker wax layer. Chapter 2 will discuss the chemical structure and dimensions involved, as well as current knowledge on the roughness of wax in subsea pipelines. Some of the text here is taken from my Specialization Project "Modeling of Wax Deposition Along Subsea Pipelines" written during the fall 2012 (Kjøraas 2012).

2.1 Chemical Structure

Crude oil consists of mostly hydrocarbons that range up to carbon numbers as high as 70 +. Crude oils consists of heavier components such as naphtenes, aromatics, resins, asphaltenes and paraffins (Singh et al. 2001). Among these the normal paraffins are the cause of wax formation, and are often found within the range of C11 to C60. This range is reported differently in the literature, but contribute to the understanding of which part of the compositional range to investigate (Kane et al. 2004).

The crystallization of paraffins is often referred to result in orthorhombic, platelet-like structures, that overlap and interlock. Compared to other components, these are said to have a strong physical interactions, which leads to the formation of a wax layer (Singh et al. 2001).

2.2 Formation of Wax layers

As mentioned in the previous section, wax crystallites often occur as platelet-like crystals. This is referred to as a result of deposition under dynamic conditions. As this is the normal condition in a field pipeline, the assumption holds. The crystallization process is complex, being governed by temperature, cooling rate, supersaturations, shear forces, impurities and paraffin carbon distribution (Singh et al. 1999). In a static environment the crystallites are said to form needle shaped crystals, and the grade of turbulence and cooling history also changes the nature of the deposited layer. The deposited layer is often seen upon as a porous layer, consisting of solid wax with entrapped oil in between. The amount of solid wax found in such a layer will depend on the thermal history as well as applied shear rates, and the composition of the crude involved.

2.2.1 Gelling of Wax Layer

When cooling of a crude containing wax components occur, the mixture will first encounter the cloud point (WAT), where wax starts to precipitate out of solution. Further cooling will result in eventually reaching the gelling point, implying that a layer with infinite viscosity, and a shear rate inside the layer equal to zero, has been established (Singh et al. 1999).

In the deposition process the cloud point will remain a thermodynamic quantity throughout, being only subject to molecular inherent properties belonging to the crude in question. The gelling temperature, on the other hand, is not a constant

parameter independent of the external environment. As noted by Singh et al. (1999) the gelation temperature would decrease with decreasing shear rate. The same trend was found when reducing the mixtures wax content, and slower cooling rates was found to hinder the network formation thus further reducing the gelation point. The shear stresses will contribute in breaking down the microstructures that bind the crystals together, and thus, the chance of gelling reduces when the shear stress increases (Singh et al. 1999).

These findings have been derived in flow-loop experiments, and needs to be under identical thermal history as well as shear rate environment before being upscaled to pipelines in the field. Often over-scaling occurs when transferring knowledge from the laboratory to real pipelines. Singh et al. (1999) found that the difference in effective cooling rate between laboratory and pipelines is around one order of magnitude higher in the field pipe, when being under similar operating conditions. This leads to over-predicting the waxy gel layer if only laboratory data is used (Singh et al. 1999).

However, gelling will not occur before the pour point of the crude is reached, which in many cases are avoided. The problem is mostly linked to start up issues after shut in, and totally blocked pipes. This section is included in the thesis due to its experimental insight on cooling rate, shear rate and wax content, and their influence on wax deposition.

2.2.2 Flow Rate Effect on Wax Deposition

Operating conditions such as flow rate has been shown to influence the deposition process. Work done by Lu et al. (2012) documented findings showing that increased flow rates tends to reduce the deposited thickness. Their analysis explained such result by comparing three different mechanism involved. Those being (Lu et al. 2012):

1. An increase in the flow rate will tend to provide a smaller boundary layer and a steeper concentration gradient, thus increasing the mass flux.

2. With a higher flow rate more oil will be pumped through the pipe, which increases the temperature at the interface. This will increase the diffusivity at the interface, and the mass flux increases.

3. By having a higher interface temperature the concentration gradient between the interface and the bulk decreases. This due to the higher amount of dissolved wax molecules at the interface.

Effects 1 and 2 suggests an increase in the deposit thickness, while effect 3 results in a decreased thickness when the flow rate is increased. Further, effect number 1 is found to be constant with respect to time, while the importance of 2 and 3 will change as time passes. The reason for this is their relationship with the interface temperature, which can change due to insulating effects posed by a changing wax layer (Lu et al. 2012).

At the initial stages of the deposition process it is believed that effect 1 and 2 dominates, while later the deposition will be a combined result of 2 and 3. By analyzing the diffusion at the oil-wax interface for different flow rates with respect to time, it is found that the importance of effect 2 diminishes with time. On the other hand, the relevance of effect 3 increases as time passes for an increased flow rate (Lu et al. 2012).

3. Challenges in Wax Deposition Modeling

Currently, a number of different methods for predicting wax deposition are used in the industry. The theory behind these models usually take on a mechanical or a chemical approach to solve the problem. However, many of the models have similarities, and often differ only in what they consider to be the most important factors constituting wax deposition. This chapter will review frequently used models, and highlight the benefits and disadvantages associated with them. Some of the text here will be a direct input from my Specialization Project "Modeling of Wax Deposition Along Subsea Pipelines" (Kjøraas 2012).

3.1 Theoretical Background

As mentioned previously, most of the analysis regarding wax deposition either takes on a mainly mechanical or a chemical approach. However, since the deposition trend is governed by both of these mechanisms one can not exclude one or the other. So the difference is mostly linked to what the authors reckon to be the most influential parameters, and also to some degree what information is at hand.

Molecular diffusion, shear dispersion, Brownian diffusion and gravity effects have all been linked to the wax deposition theory. Molecular diffusion is seen as the most important, and is therefore included in almost all present models. The importance of shear dispersion has in later years been questioned by various authors (Siljuberg 2012; Gudmundsson 2010). Brownian diffusion and gravity effects are often seen as less important. The main difference between molecular diffusion and shear dispersion is that molecular diffusion transport wax which is in solution, while shear dispersion consists of a wax transport of already precipitated wax particles (Bern et al. 1980).

3.1.1 Molecular Diffusion

Molecular diffusion acts as soon as the pipe wall temperature reaches the WAT, and wax precipitate out of solution. This precipitated wax creates a concentration gradient between the amount of dissolved wax at the pipe wall and the wax remaining in solution in the bulk fluid (Bern et al. 1980). This concentration gradient leads to diffusion of dissolved particles from the bulk to the wall, and a subsequent precipitation at the wall due to the fact that the temperature is below WAT at this location. The somewhat rough surface of the pipe wall creates an ideal nucleation site for the precipitated wax particles and a deposit is likely to form. The molecular diffusion is often represented physically by Fick's diffusion equation (Bern et al. 1980):

$$n = \rho D \frac{dC}{dr} = \rho D \frac{dC}{dT} \frac{dT}{dr} \tag{3.1}$$

Where ρ is the density, D is the diffusivity constant, $\frac{dC}{dr}$ is the concentration gradient and $\frac{dT}{dr}$ is the temperature gradient between the bulk and wall.

Further, molecular diffusion will be closely linked to the radial temperature gradient, and will continue as long as there is a change between the temperature in the bulk and the pipe wall. In a practical sense this means that the rate of molecular diffusion will be at its maximum just below the WAT and then gradually decrease as the temperature falls to a steady state temperature across the radial profile of the pipe.

3.1.2 Shear Dispersion

Shear dispersion is the mechanism that lead already precipitated wax particles in the bulk fluid to deposit on the pipe wall. Normally precipitated particles will tend to move in the direction of the flow itself, however, close to the pipe wall shear effects may succumb the particle to laminar flow. Traditionally this has led to the belief that particles will move towards the wall, and adjoin to the existing wax deposit. However, information presented in later years has suggested otherwise. Arguments

that a particle found in the sublayer are subject to a lift force, due to lower pressure acting on the top side of an particle, suggests that particles dissolved in the bulk most likely will not settle on the wall (Siljuberg 2011). Other reports presented in the literature, divides the deposition process into three regimes. The first regime is totally governed by turbulent diffusion, the second is subject to turbulent eddy-diffusion impaction and regime three is particle inertia governed (Guha 2008). These three regimes are indirectly linked to the size of the particles, due to their different relaxation times, where small particles generally fall under the deposition trend in regime one, namely diffusion.

3.1.3 Other Effects

The previous mentioned fluid mechanisms describes how the wax might form a layer on the wall, but the situation is not constant even after the deposit is created. Effects such as shear removal and aging will influence the thickness and are factors that further complicates the modeling of a potential wax problem. Shear removal refers to a situation where wax is torn off as a result of high shear stress at the liquid-solid interface. The process where wax molecules diffuse into an already existing wax layer or when oil dissipates out and into the bulk flow again, or both, is called aging. Since the deposition is not only described by a single factor, it poses difficulties distinguishing the controlling factors and a refined sensitivity analysis is therefore needed. This will not be conducted in detail in this report, since it falls outside the scope of the hypothesis.

3.2 Models

3.2.1 Deposition Release Model

The deposition release model is a semi-empirical model, where experimetal values are implemented in the model. Gudmundsson has presented such models, which

Botne investigated further in his specialization project, and later in his master thesis (Botne 2012, 2011). The semi-empirical deposition release model was suggested as a reasonable approach to the modeling of wax thickness. This model states that the growth of deposit thickness is equal to the rate of deposition minus the rate of removal:

$$\frac{dx}{dt} = x_D - x_R \tag{3.2}$$

Botne conducted several simulations on this model, which can be evaluated as either an exponential or a logarithmic expression. The results from these were compared to experiments done by Rosvold (Rosvold 2008), and Singh et al. (Singh et al. 2011), and found to give a reasonable match. It was shown that the logarithmic model displayed somewhat better results.

Exponential Model (Gudmundsson 1981):

$$\frac{dx}{dt} = k_1 - k_2 x \tag{3.3}$$

Logarithmic Model (Gudmundsson 2010):

$$\frac{dx}{dt} = k_1 k_2^{-x} \tag{3.4}$$

k_1 and k_2 are constants, and are explained further in Botne's master thesis (Botne 2011).

The deposition release models use an initial deposition rate and a maximum deposition thickness as a function of time in their analysis of wax deposition (Botne 2012). The essential difference between the exponential and the logarithmic model is how these constants are evaluated and combined in order to represent wax deposition. For the logarithmic model it is not necessarily experienced to reach the asymptotic level of wax thickness, but the rate of deposition will be significantly reduced compared to the build up period.

3.2.2 Pressure drop

More conventional wax models include the standard pressure drop method, where recorded or calculated pressure drop can relate the deposit thickness relative to a clean pipe. The pressure drop method consist of several parameters that can be seen upon as constant along the pipeline, such as the density of the fluid and the pipe length. In many cases the flow rate is kept constant as well, leaving the changing parameters to be the pressure drop, Reynolds number and the diameter.

The standard Darcy-Weisbach for frictional pressure drop is presented as the following equation (Gudmundsson 2009):

$$\Delta p = \frac{f}{2}\frac{L}{d}\rho u^2 = \frac{f}{2}\frac{L}{d}\rho(\frac{4q}{\pi d^2})^2 = \frac{8f}{\pi^2}\frac{L}{d^5}\rho q^2 \tag{3.5}$$

The parameters used in this equation are as follows: L (m) distance along pipe, d is the diameter (m), ρ (kg/m^3 the density, f is the friction factor, u (m/s) the velocity and q (m^3/s) is the flow rate.

3.2.3 Temperature Drop

Modeling the temperature difference would also work well when trying to find the deposition thickness (Hoffmann and Amundsen 2009). If the thermal conductivity of the deposited layer were known, this could be used to calculate the thickness by evaluating the temperature drop. However, it has been shown that thermal conductivity strongly relates to the wax content of the deposited layer which complicates the use of this method. As stated earlier the wax layer is subject to a phenomenon referred to as aging, which leads to a continuously changing thermal conductivity.

3.2.4 Film Penetration Model

The literature refers to two different ways of transferring mass and heat, namely the film theory and the penetration model (Toor and Marchello 1958). In earlier years these two models have been thought of as independent. Now, these models are thought to both influence the transfer mechanism, but at different times. The penetration gives a name to the process where the interface is continuously replaced by eddies which makes this an unsteady state molecular transfer. The film theory, on the other hand, assumes that there is a region where steady state molecular transfer is achieved. The authors of the article "Film Penetration Model for Heat and Mass Transfer" (Toor and Marchello 1958) conclude that for low Schmidt numbers the film theory will prevail, while for higher Schmidt numbers the penetration model will be the most dominant mechanism. For intermediate numbers both mechanisms will describe the transport, and the situation will be of a more complex nature.

The film mass theory has been used to describe the deposition trend in many articles, among them "Morphological Evolution of Thick Wax Deposits During Aging" by (Singh et al. 2001). The film mass model describes a gel that consists of wax that interlocks and contain trapped oil. Initially, a thin-film model was used to describe the deposited layer. This thin layer was assumed to have a radially uniform composition, that is, the molecular diffusion will behave identical throughout the entire radial thickness. For a thin layer the characteristic diffusion length of the wax molecules are of the same order as the layer itself, and the diffusion will thus occur uniformly (Singh et al. 2001).

Later, a thick-film model has been investigated. In thicker wax-layers the diffusion length is found to smaller than the thickness of the layer, which results in an uneven composition distribution. To illustrate this, one can assume that such a layer will age differently in the radial direction (Singh et al. 2001). For both the thin and the thick layer the diffusion results from a concentration gradient, where an interface of different concentration either exists on the oil-wax interface for a thin layer, or throughout the thick layer in addition to the interface. Experiments done confirms

these assumptions by showing that thick layers have a higher wax content in the near interface region compared to the region close to the wall (Singh et al. 2001).

3.2.5 Equilibrium Model

Another thermodynamic model uses the vapor-liquid and solid-liquid equilibrium to establish phase equilibria with a possible chance of wax formation (Elsharkawy et al. 1999). This equilibrium model is based on calculations of fugacity. Fugacity is an effective pressure that replaces the mechanical pressure when a gas or liquid is in total chemical equilibrium. The fugacity expresses the tendency to either expand or escape.

$$f_i^S = x_i^S \phi_i^{oL} p \cdot exp[\frac{-\Delta H_i^f}{RT}(1 - \frac{T}{T_i^f})] \tag{3.6}$$

where the liquid phase fugacity, ϕ_i^{oL} can be found from Soave-Recdlich-Kwong (SRK) equation of state for pure components. The x is the phase mole fraction, p pressure, ΔH represent the enthalpy of fusion, R is the universal gas constant while T and T_i^f is the temperature and melting temperature respectively (Elsharkawy et al. 1999). To account for possible wax formation, information regarding melting temperature, enthalpy of diffusion and molar volume needs to be established before using this method. This model solely predicts the precipitated wax components, more than the wax deposition itself.

Solid wax will only crystallize when the mixture is supersaturated. If this happens close to the wall interface, then the crystals will most likely settle on to the wall or adjoin an already existing wax layer. However, if the supersaturation occurs in the center of the pipe the precipitated crystals may be carried by the turbulent flow to a location that does not satisfy supersaturation. Here, the crystals might disintegrate and become a part of the solute once again (Bott 1997).

3.2.6 Discussion

The models presented are the pressure drop and temperature models, deposition release models and thermodynamic models. The pressure drop and temperature drop method conducts their analysis on the basis of already deposited wax layers. By means of reduced pressure measures or higher insulating effects, these models can calculate the thickness of the wax layer. The film mass transfer uses primarily diffusion in the prediction, while the equilibrium model solely evaluates a potential for the deposition based on the crudes inherent precipitation characteristic.

However, an ideal model would need to incorporate all of these physical and chemical properties. The equilibrium model present useful insight regarding when crystals might start to precipitate, and gives the precipitation curve as the environment changes. Information about which components that most likely will contribute to a wax layer, at a given point, would be beneficial when the predicting is done by an analysis of heat transfer. The film mass transfer model, in combination with the equilibrium model, would be suitable for this. When all this is done, the pressure drop method would be well used to confirm the predictions. It is then perhaps, as often reported in literature, logical to expect a thicker layer calculated by the pressure drop analysis than the other combined models. This, due to possible roughness effects of the deposited surface.

4. Roughness

A frequently used method to quantify wax thickness in field pipelines are by use of a pressure pulse technology. By relating the pressure pulse of a wax inflicted pipe to the results from a clean pipe, the thickness profile can be found. However, as discussed previously this technique is limited by the uncertainty linked to the roughness of the deposited wax layer. In the literature on wax deposition the inclusion of roughness is evaluated differently, from not including it at all, to assigning great importance to it. Several reports suggest that the roughness grows in the same order as the thickness up to a upper limiting value (Rønningsen 2012). This chapter will try to discuss and present the current knowledge on roughness, and some of the information will be used in combination with simulation results from FLUENT in Chapter 7.

4.1 Approaches to Roughness Quantification

Usually, the roughness factor is evaluated as a tuning parameter. If modeling flow through a pipe subjected to wax settlement is to be evaluated correctly, more investigation regarding the roughness is needed. Useful information include parameters such as the asymptotic upper limit of wax roughness, and the shape of the deposits as this is said to affect the pressure drop.

Since little visual evidence exists on the shape and size of wax layers, other methods to describe the physical environment needs to be looked into. Possibly, investigations into the crystallization process and entropy state of wax deposition processes might give some insight on the topic. Chemical, thermal and flow effects will then all contribute to the resulting shape and size of a wax layer. However, in this thesis only the pure mechanical approach will be analysed.

Most literature found in combination with this thesis, focuses more on determining the roughness effect by assigning the deviations between measured and calculated

pressure drop, to be roughness effects. Further, the norm is to quantify this extra friction term by use of solely roughness height. Such models, in addition to a model that includes the geometrical shape of the rough deposits, will be presented in the subsequent chapters.

4.1.1 Baumann and Rehme Model

Research done on different types of roughness environments, shows that the friction factor alternates with structural changes. Roughness resulting from an uniformly distributed roughness, such as sand grain roughness, differs from a structured deposit, such as rippled or rectangular surfaces (Gudmundsson 2010).

One of the first approaches to include roughness effects was presented by Prandtl, and investigated further by Nikuradse. It is the work done by Nikuradse that will be presented in this thesis. Nikuradse presented an analogy based on thigthly packed sand grains. This analysis only included the roughness height in the calculation of the resulting friction factor. However, it is believed that the results from Nikuradse's equation will give misleading results for roughness environments that deviate from the shape of packed sand grains. Nikuradse's model will be further discussed in the next subschapter.

A model used to describe the effects of a rectangular roughness environment on the roughness function was suggested by Baumann and Rehme (Baumann and Rehme 1974):

$$\sqrt{\frac{8}{\lambda}} = 2.5ln(L/h) + R - G \tag{4.1}$$

In Equation 4.1 the friction factor is denoted as λ and is of the same form as Darcy-Weisbach's friction factor, L is the length of the velocity profile between the wall and the zero-shear position (the radius of a pipe in pipe flow) and h is the height of the roughness element. G is a geometry parameter, found to be equal to 3.75 for

circular rough tubes (Maubach 1970), while the roughness parameter R is a function of the roughness geometry.

Baumann and Rehme discussed the difficulties connected with describing and relating friction factors resulting from different roughness environments. They put forward an analysis that arrived in the relationship presented in Equation (4.1). To achieve this they normalized different geometries with respect to an h/L relationship. By doing this they arrived to the following equations needed to describe the roughness function, R:

1. Roughness parameter R_0 transformed for $h/L = 0$:

$$R_0 = a_1(\frac{p}{h})^{a_2} + a_3(\frac{p}{h})^{a_4} \tag{4.2}$$

TABLE 4.1: Constants

$a_1 = 18.5(\frac{h}{w})^{-0.9475}$
$a_2 = -1.143(\frac{h}{w})^{-0.147}$
$a_3 = 0.33(\frac{h}{w})^{0.1483}$
$a_4 = 0.758(\frac{h}{w})^{-0.11}$

TABLE 4.2: Limits

$1 \leq \frac{p}{h} \leq 40$
$0.3 \leq \frac{h}{w} \leq 8$
$\frac{h}{L}$
$R_0 \leq 10$
$h^+ = \frac{hu^*}{\nu} \geq 100$

Where the four constants are described by the height (h), width (w) and pitch (p) of the deposited surface, as well as experimentally developed values. h^+ describes the dimensionless roughness height, or sometimes called the roughness Reynolds number. It is required to be greater than 100 to assure that the situation can be seen as fully rough.

2. The dependence on the ratio between the height of roughness and the length of the velocity profile is described below:

$$R_{k_1,k_2} = 2.900 + 1.490(\frac{h}{L}) - 1.972(\frac{h}{L})^2 \tag{4.3}$$

The Least Square Fit-approximation used by Baumann and Rehme has its maximum when $h/L = 0.38$, which is the origin for the equation presented above.

3. The dependence of the roughness parameter to the relative height of roughness h/L when incorporating a 3. fictitious R_0 for $h/L = 0$:

$$R_{k_1,k_2} - R_{0_{k_1,k_2}} = \sum_{k=2}^{n} z_k(\frac{h}{L})^{k-1} \tag{4.4}$$

This relationship has the same origin as equation 4.3, which gives a $R_{0_{k1,k2}} = 2.9$ for all geometries.

4. Resulting from the above derivations is the roughness parameter for a given h/L:

$$R = R_0 + \frac{R_0}{R_{0_{k_1,k_2}}}(R_{k_1,k_2} - R_{0_{k_1,k_2}}) \tag{4.5}$$

When the roughness parameter R, a result from equation 4.5, is entered into equation 4.1, the friction factor can be calculated.

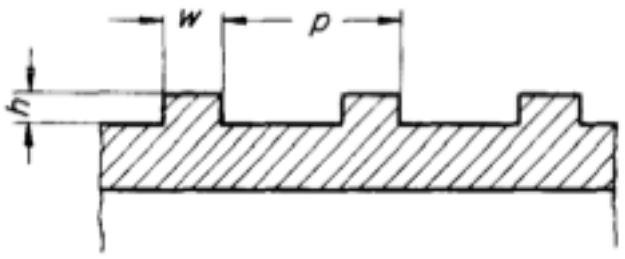

FIGURE 4.1: Rectangular Roughness Geometry

Baumann and Rehme's equations will be used to calculate friction factors for the different cases presented in this text, however, the results will be presented in chapter 7. The results will be compared to results obtained by simulations in FLUENT, and calculations on Nikuradse's equation for sand grain roughness.

4.1.2 Nikuradse

As previously mentioned, Nikuradse was one of the first to include the roughness effects on the friction factor. To quantify the roughness effect Nikuradse (1933) presented a relationship called a roughness function, which can also be used to calculate the friction factor (Gudmundsson 2010):

$$B = \sqrt{\frac{8}{f}} + 2.5ln(k/r) + 3.75 \tag{4.6}$$

This expression is based on an analogy between the roughness of tightly packed sand grains, and how this can be used to describe a rough surface. The roughness factor B was experimentally determined by Nikuradse and divided into three different definitions, based on an dimensionless roughness height (Nikuradse 1933) (Gudmundsson 2010):

$$k^+ = \frac{\rho u^* k}{\mu} \tag{4.7}$$

Where ρ is the density, u^* the friction velocity, k roughness height and μ stands for the viscosity. The three different regions are:

- **Smooth Surface**: B=5

$$0 \leq {k_s}^+ \leq 5 \tag{4.8}$$

- **Intermediate Rough Surface**: B is a function of ${k_s}^+$.

$$5 \leq {k_s}^+ \leq 70 \tag{4.9}$$

- **Fully Rough Surface**: B=8

$$70 \leq {k_s}^+ \tag{4.10}$$

This model will be used in calculations done in this report, where results can be found in chapter 7.

4.2 Roughness Quantification of Wax Deposits

As stated previously, most attempts to include roughness effects in connection with wax deposition has been incorporated through defining a likely roughness height. The information brought up in this section is mainly included to justify the importance of a roughness quantification of wax in pipelines.

In a master thesis written by Handal (2008), a similar expression of Nikuradse dimensionless roughness height was presented, but evaluated as a function of the kinematic viscosity and shear velocity in the wall region (Handal 2008):

$$k_s^+ = \frac{u_\tau k_s}{\nu} \tag{4.11}$$

Handal conducted experiments based on the assumption that the roughness should change very little during the experiments, which implies that the roughness changes immediately from a zero roughness to a constant value related to the deposition (Handal 2008). This can be related to the assumption that the roughness will stop growing when it reaches an upper limit. Another important aspect is the fact that the pipe used needs to be hydraulically smooth in order to be able to describe the situation mathematically. Handal evaluated three different constant roughness heights, and found that an increase in roughness seemed to lead to a decrease in

deposit thickness. Further, in the initial period of the experiments a negative deposit thickness was observed. This information was extrated from an analysis done on heat transfer. When including a constant roughness height, and then increasing the roughness further this resulted in an even thinner deposit (Handal 2008).

To account for this Handal tested a hypothetical roughness height function, given below (Handal 2008):

$$k_s = A(1 - exp(-bt)) \tag{4.12}$$

This equation describes the roughness height by an asymptotic level, A, and a time variable, b, that states the build up time for the wax structure. The equation above is found in Edmonds et al. (2008) in their modeling of deposit in light of the size of deposit minus the rate of removal. This model was put forward as a result of the evidence relating to the tendency for a wax layer to reach a plateau with time (Edmonds et al. 2008). The tendency of shearing off the waxy gel investigated in Edmonds paper, by forces applied by the flowing fluid, resulted in the following representation for wax thickness build-up:

$$x = A - B(1 - exp(-Ct)) \tag{4.13}$$

This expression can be linked to Gudmundsson's exponential deposition release model (Gudmundsson 2010), which Botne further investigated in his specialization project in 2011.

Collected data from full scale operations concerning increased wall roughness can be found in the investigation done in connection with the extensive cleaning of the Valhall pipe system (Marshall 1988). Even though there are uncertainties in the findings, the author still conclude that there are enough evidence to support a build up of roughness which affects the pressure drop along the pipe. At one point the calculated roughness showed to be bigger than the thickness of the solid itself, which would indicate a very rough surface.

Experimental data from Hoffman and Amundsen (2009) also suggest that unlike conditions can have an impact on the resulting wax deposition. This result was found by varying the flow rate for very short times and in small steps, which would not affect the deposition rate in a significant way, leaving the changes from this to be a result of roughness environment (Hoffmann and Amundsen 2009) .

In the work done by Edmonds et al. (2008) in " Simulating Wax Deposition in Pipelines for Flow Assurance " it was found that by calculating the pressure drop (regardless of the friction factor used) for an observed wax thickness, the results should be less than twice that for a bare pipe. However, the measured pressure drop was higher than this, leaving this increase in pressure drop unexplained (Edmonds et al. 2008). A possible reason for this might be roughness effects, since the pressure drop is highly affected by this property.

The study by Venkatesan et al. " Formation and Aging of Incipient Thin Film Wax-Oil Gels " an X-ray diffraction analysis investigated the thickness of a multi-component paraffin wax crystal, and found that this was equal to the average length of the wax molecules in the mixture. The same study also found that the effective diffusion of wax molecules into the wax layer was a function of the average aspect ratio of the wax particles, and that this property was reduced by applied shear stress (Venkatesan et al. 2000).

Reports from Guha [2008] regarding deposition, showed that the presence of even very small roughness elements, would enhance the deposition trend significantly. This effect was especially relevant when the deposition process involved small particles (Guha 2008). This knowledge, together with some of the reports presented above, clearly show that roughness affects the wax deposition process.

4.3 Roughness and Heat Transfer

Baumann and Rehme reported that roughness at the wall would not only increase the heat transfer, it would also lead to higher losses of pressure. The increase in

heat transfer is essentially linked to the increased turbulence effect due to enhanced roughness (Baumann and Rehme 1974).

Reports such as the one from Donne and Meyer (1977), states that artificial roughness do in fact contribute to an improvement of heat transfer. They investigated an artificial roughness, built from cladding graphite which acted as a promoter of turbulence. This would at the same time interrupt the viscous sublayer, which is located adjacent to the wall (Donne and Meyer 1977). This led to an increase in both the friction factor and the heat transfer. They further divided the ruling geometry into two main regimes, namely a microscopic and macroscopic geometry. The microscopic being parameters created by the rough surface, that is the height of roughness element, width and pitch between subsequent elements. The macroscopic geometry was related to the environment that dictated the flow regime on a bigger scale, those being for example tube, annulus or rectangular channels among others.

To evaluate the heat and momentum transfer cross a rough surface, a correlation between a smooth and rough regime is often used. In order to describe effects one often compares the results from a rough regime against the results obtained for a smooth environment. Dipprey and Sabersky (1963) conducted such an analysis, and derived a relationship for the Stanton number (St) for a smooth flat plate (Webb and Kim 2005).

$$St_s = \frac{f_s/2}{1.0 + 12.7(f_s/2)^{1/2}(Pr^{2/3} - 1)} \tag{4.14}$$

Webb (1971) showed that for flow in smooth tubes 1.0 should be replaced with 1.07. The f_s is the friction factor for the smooth case, and Pr is the Prandtl number. For this purpose Petukhov (1970) recommends that the following friction factor should be used for the smooth case (Webb and Kim 2005):

$$f_s = (1.58 ln Re_d - 3.28)^{-2} \tag{4.15}$$

The same analogy for the Stanton number has been developed, and is presented as follows (Webb and Kim 2005):

$$St = \frac{f/2}{1 + \sqrt{f/2}[\bar{g}(e^+)Pr^n - B(e^+)]} \tag{4.16}$$

where Pr^n is equal to $Pr^{0.44}$, $g(e^+)$ can be read from a figure based on $g(e^+)$ plotted against the dimensionless roughness height. $B(e^+)$ can be found by reading values from a graph of $B(e^+)$ plotted against the logarithm of the dimensionless roughness height (Webb and Kim 2005). The friction factor presented in equations 4.14 through 4.16 are the Fanning friction factor.

5. Simulation in FLUENT

ANSYS Technology's software Fluent enables users to calculate flow specific parameters, and is therefore well suited to the tasks at hand in this thesis. The theory presented in this chapter is found from the Fluent User Guide and in the Fluent Theory Guide (ANSYS Inc 2009c,a). In addition to this the Fluent Tutorial Guide have been used for help and guidance during the set up and running of simulations (ANSYS Inc 2009b).

5.1 Theory

The aim of the simulations are to model the effects roughness have on the pressure drop, and compare the results to earlier findings in the literature. As mentioned numerous times previuosly, a rough element is believed to induce a higher pressure drop compared to a smooth scenario. This is well known knowledge, however, the full effects of the roughness environment is yet not fully understood. The simulations conducted in this thesis will include three different roughness environments. Those being rectangular deposits, rippled deposits and equivalent sand grain deposits, which will be explained in detail later in this chapter.

The results will be compared in terms of the friction factor. The simulations will give rise to a pressure drop, which will be used to calculate the friction factor. For the simulation results, the Darcy-Weisbach equation will be used:

$$\Delta p = \frac{f_D}{2}\frac{\Delta L}{d}\rho u^2 \tag{5.1}$$

where f_D is the Darcy friction factor, ΔL is the length where the pressure drop is analyzed over, ρ is the density of the flowing medium and u is the velocity.

The results will be compared to calculated friction factors, such as the one Baumann and Rehme (Baumann and Rehme 1974) suggested, as well as the friction factor coming from Nikarudse's sand grain roughness (Gudmundsson 2010). This comparison will be found in Chapter 7 and Chapter 8.

5.2 Physical Model

There are various models that can be used to model flow through a pipe in FLUENT. Depending on the governing environment, and which parameters that is to be investigated, the simulation can be tailored differently. In FLUENT, the conservation equation for momentum and mass will be solved for all flows. If the flow includes heat transfer or compressibility the software will solve the energy conservation equation as well. For flows of turbulent nature, there will be additional equations, such as various transport equations.

Table 5.1 shows the physical equations used in simulations conducted in this thesis. The equations for momentum, mass and energy are standard equations, and will therefore not be explained here, but can be found in the Theory Guide (ANSYS Inc 2009a). FLUENT offers three choices for solving the turbulent equation. Those are the standard, RNG, and realizable turbulent equation. In this thesis the RNG turbulence model has been chosen, due to its ability to handle abrupt changes in the flow pattern. It is also possible to define a near wall treatment method, and for these simulations the Enhanced Wall Treatment has been chosen for the Cavity Induced Roughness, while the Standard model has been chosen for the Wall Treatment Roughness. Both Wall Treatment and Cavity Induced Roughness will be further explained later in this chapter.

TABLE 5.1: Physical Model

Property	Action
Momentum	Automatically
Mass	Automatically
Energy	Turned ON
Turbulent Equation	RNG k-ϵ
Near Wall Treatment	Enhanced Wall Treatment/ Standard

5.3 Procedure

There are different types of roughness regimes reported in literature, however, little knowledge exists on which regime is likely to be found in connection with wax deposition. Therefore, this report will include simulations on different types of roughness, and different roughness heights.

The simulations will be conducted in two fundamental different ways.

1. Wall Treatment Roughness: FLUENT has a predefined method to incorporate roughness effects. This method uses input values of the roughness height, k_s, and a roughness constant, C_s. The roughness constant aims to describe the roughness environment. The disadvantage induced by using this method is that the roughness constant is practically not defined at all. The parameter, C_s, is defined to be equal to 0.5 for sand grain roughness, and it is known that values above this represents a roughness regime that is non-uniform. It is further said that the value is normally within 0.5-1. Outside this, there exists little information about the parameter. Another restriction relates to the roughness height, and the need for k_s to be less than half of the mesh cell adjacent to the wall to avoid disturbing the calculation. It is possible to decrease the meshing intensity near the wall, but this might result in a less accurate result. Therefore, the maximum roughness height has been set to $k_s = 0.55$, to achieve the most optimal result with the mesh used.

2. Cavity Induced Roughness: The other way to simulate roughness effects is incorporated by constructing the pipe geometry to be rough in itself. This is done by creating obstacles along the internal pipe wall. These obstacles are either rectangular or rippled in shape. The rippled obstacles consists of a half circle and a vertical line, resembling a wave front. The height and width is varied in both cases. The disadvantage connected with this approach was that it was not succeeded to construct a geometry with a smooth outer surface and a rough inside. This limits the possibility for correct heat transfer information, since the roughness elements does not impose a thicker solid region. This limitation is due to time- and skill limitations of the author of this text.

Table 5.2 show the cases run with the inherent roughness treatment option in FLUENT. It is run for three scenarios, an equivalent sand grain roughness, a completely non-uniform scenario and for a scenario in between.

TABLE 5.2: Wall Treatment Roughness

	Sand Grain Roughness $Cs = 0.5$	Non-Uniform Roughness $C_s = 0.75$	$C_s = 1$
$k_s = 5.5$	Case A	Case B	Case C
$k_s = 2.5$	Case D	Case E	Case F

TABLE 5.3: Cavity Induced Roughness

	Rectangular Roughness	Rippled Roughness
$h = 5.5$ $w = 14$ $p = 56$	Case G	Case H
$h = 2.5$ $w = 14$ $p = 56$	Case I	Case J
$h = 5.5$ $w = 14$ $p = 35$	Case K	Case L
$h = 2.5$ $w = 5$ $p = 52$	Case M	Case N

Table 5.3 is an overview of the cases run on Cavity Induced Roughness. Table 5.4 show some additional cases, which acts as a reference to the cases presented in table 5.3 for various reasons. Case G/H and I/J will be compared to see the effects of

varying roughness height. Case G/H and K/N will be compared to investigate the effects of the distance between the rough elements, while Case M/N is provided because Case I/J fall outside the limits in Baumann & Rehme's model.

Table 5.4: Reference Cases

Smooth Wall	Case O
Baumann & Rehme	Case P
Enlarged Diameter	Case Q

Since these simulations only has the aim to investigate the effects of roughness, it has been concluded that it is sufficient to run the simulations with water as the flowing medium. However, as soon as one wants to model, for example, how heat transfer in wax deposition is affected by a roughened environment one obviously needs to replace water with oil. Most of the simulations are conducted on a much smaller scale than a realistic transport pipe system. This mainly due to stability issues related to achieving a fully developed velocity profile before entering the rough section, as well as stability requirements within the rough section itself. However, one case is simulated with full scale dimensions in order to check the effects this might have on the resulting pressure loss. Table 5.5 shows the input parameters for most of the simulations.

Table 5.5: Input Values

	Property	SI
Wall Treatment Roughness	Length	5
Cavity Induced Roughness	Total Length	8
Cavity Induced Roughness	Rough Section	6
	Radius	0.018
	Wall Thickness	0.005
	Entrance Velocity	2
	Operating Pressure	101325
	Temperature	300
	Turbulence Intensity	4
	Hydraulic Diameter	0.036

The solution in FLUENT is reached by following a predefined structural setup.

1. **Geometry:** The initial step include defining the geometry in question. Flow through a circular pipe is generally constructed as a rectangular box, where the height of the box signifies the pipe's radius. In addition to setting the radius and the length of the pipe, the user is asked to define the wall thickness. The rectangular area will later be reflected about a defined axis, in order to portray pipe flow.

2. **Mesh:** Step two involves the construction of an appropriate meshing structure. The accuracy and quality of the mesh is often very important, however, it also poses difficulties due to conflicting interests. A good mesh should be composed by cells small enough to calculate the solution to the required accuracy, and it should be as uniform as possible throughout the domain. Meshing limitations is generally linked to time consuming simulations, and mesh cells that is smaller than the minimum allowed mesh cell. Here, the mesh has been a result of achieving the most accurate cells near the roughness elements, without crossing the minimum allowed cell size, and a big enough mesh to be able to handle the calculations.

3. **Setup:** After the meshing operation, all the model parameters are defined in the Setup box. This includes defining the governing models, and defining the operating conditions such as velocity and turbulence parameters.

4. **Solution:** Before simulation can be run in the solver, the user needs to define monitor levels that tells FLUENT when a sufficient limit of convergence has been reached. These limits are set according to the parameters that are included in the model, for example, turbulent dissipation rate, turbulent kinetic energy and momentum. The convergence limits are set to $1 * 10^{-6}$, which is usually seen upon as sufficient for most cases. The final step before conducting a simulation is to initialize the solution with respect to the defined entrance region, in this case the pipe inlet.

5. **Results:** The final step is the result box, where the calculated values are being post processed. FLUENT offers two possibilities for post-processing, either directly in FLUENT, or as a separate post-processing program launched from the Workbench. Both arrive at the same result, however, the separate post-processing tool is somewhat more user-friendly and simple to handle.

The results of the simulations run is presented in Chapter 7: Results.

6. Friction Factor

Chapter 6 is included to gain insight on possible effects on the friction factor resulting from the different geometries investigated in this report.

The geometries tested is rectangular, wedge-shaped (ripples) and sand grain deposits. The main focus lies on the investigation of rectangular and rippled surfaces.

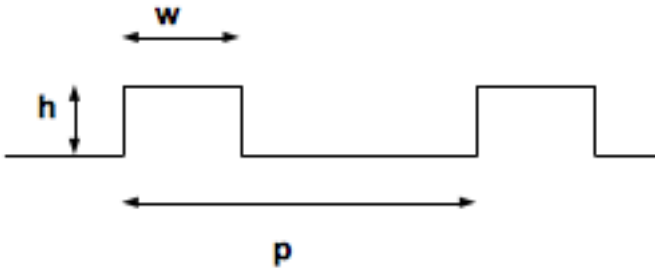

FIGURE 6.1: Rectangular Roughness Elements

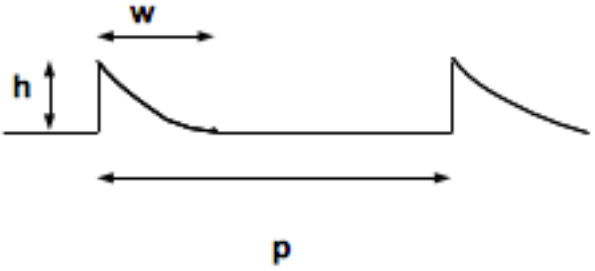

FIGURE 6.2: Rippled Roughness Elements

FIGURE 6.3: Sand Grain Roughness Elements

These three geometries has been chosen due to various reasons. Rectangular roughness is probably very unlikely to be found in connection with wax deposition. However, since very litte investigation has been done on a wax layer roughness' information from other areas has been used. The sources of information is generally found in connection with heat transfer investigations. In this area the aim is to assure, or avoid, high heat transfer, while at the same time prevent the pressure drop to become too high. It is difficult to say which kind of roughness environment will exist in wax deposition, and if the shape of it is general or independent of each wax deposition history. However, one possible geomtery might resemble the shape of ripples, and is therefore included in this thesis. The sand grain analysis is included because it is a widely accepted method to incorporate roughness effects when calculating the friction factor.

The existence of rough elements in a pipe results in an additional pressure drop. This is a result of the extra drag created by the interaction between the flowing fluid and the rough elements. The roughness elements changes the flow picture around them, and thus alters both the drag resistance and the shear stress acting on the wall (Su 1996).

All cases presented in the previous chapters belong to the group of roughness elements named protrusions. For portrusions it is generally accepted that the ratio of protrusions, that is the roughness height, to the boundary layer thickness is a determinating factor. Results from Nikuradse's measurements showed that for a fully rough flow, the friction factor was independent of the Reynolds number. Leaving the controlling determinant to be the ratio of roughness height to the radius of a circular pipe, k/R. Since all cases run in connection with this report can be seen as fully rough, results can be expected to be governed by the k/R relationship.

Webb and Kim (2005) contributes to the insight of flow past rectangular rough elements. They states that the flow will separate when subject to a rough element protrusion. However, reattachment will occur at certain distances past the rough element. Webb and Kim states that the reattachment will occur at lengths between 6 to 8 times the roughness height(Webb and Kim 2005). Knowledge about how the

fluid will separate and later reattach, present insight into possible effects on having varying distances between the rough elements. For example, case G ($h = 5.5mm, p = 56mm$) will experience reattachment, while Case K ($h = 5.5mm, p = 35mm$), will most likely not.

In Ze Su's doctorate dissertation different classifications of roughness elements are presented (Su 1996). Two types relating to pipe flow, and the cases run in this report, is K- and D-type. A K-type roughness is defined to exist when the friction factor and Reynolds characteristics are sensitive to the relative roughness k/R. The D-type is defined for pipe flow where the roughness function is not dependent on the roughness height, but the pipe radius alone. This relationship was presented by Perry et al. (1969), but it is referred to again in Su (1996). It is stated that a D-type roughness environment exhibit roughness elements that are more closely spaced. In such situations, there will be stable vortices in the grooves between the rough elements, and eddy shedding from the elements into the flow can be considered negligible (Su 1996). This phenomenon might be relevant for the case with $p = 35mm$.

Webb and Kim (2005) reports that the roughness height should be around seven times bigger when analyzed through the sand grain analysis, compared to 2D rectangular roughness height, if the same friction factor is to be obtained. Bott and Gudmundsson (1978) also reported the same trend, though for rippled roughness. These findings also showed that the friction factor decreased with increasing Reynolds numbers, which contradicts the findings of Nikuradse stating that the friction factor is independent of Reynolds number for a fully rough regime (Bott and Gudmundsson 1978).

Webb and Kim (2005) also investigated the effect of having rounded edges compared to sharp shaped boxes, and found that the rounded scenario resulted in a decreased friction factor. This does not directly affect any of the cases run in this report, since the rectangular roughness is only simulated with sharp edges. The rippled roughness might be seen in light of having rounded edges, however, there are two many other contributing factors that it is difficult to link this to the resulting friction factor.

From the information presented in this chapter, one would expect significantly higher results of the friction factor for rectangular and rippled roughness compared to sand grain roughness simulated with the Wall Treated function in FLUENT. Further, rippled deposits is reported several times to give higher friction factors than rectangular roughness.

Another important aspect, the relationship between the roughness height and the radius of the pipe is referred to as a controlling factor by both Webb and Kim (2005) and Su (1996). In this report most of the cases are run with a very high k/R relationship, that is a relative high roughness height compared to a small radius.

7. Results

This chapter will present the results obtained in this thesis. It will in the first part show the results gained by calculation, then the simulation results will be presented. The results will be compared and discussed in Chapter 8.

7.1 Baumann and Rehme

Table 7.1 and 7.2 shows the calculated results for the friction factor using Baumann and Rehme's method. Both tables shows each of the four steps needed before calculating the friction factor, as explained in section 4.1.1.

TABLE 7.1: Calculation Results Rectangular Roughness (Baumann and Rehme 1974)

Case	R_0	$R_{k1,k2}$	$R_{0_{k1,k2}}$	R	f
G	4.2	3.17	2.9	4.55	0.566
I	-	-	-	-	-
K	5.3	3.17	2.9	5.82	0.316
M	4.3	3.07	2.9	4.58	0.240

All of the presented cases in table above are within the presented limits posed by Baumann and Rehme, however, as can be noted the results of the friction factors are quite high. As far as the author of this text knows, it is not normal to achieve friction factors in this range, at least not for the interaction between a liquid and a solid. A possible reason for these results, may very well be that the roughness elements are too high in relation with a too small diameter. However, a clear definition on the limits of h/L has not been successfully found in the literature.

By taking a look at table 7.2, somewhat different results can be seen. Table 7.2 consists of an example case given in Baumann and Rehme's paper, and, a case of

similar roughness elements but with a larger diameter compared to the presented cases in table 7.1. These values resembles values of the friction factor too a much greater extent. However, yet again both tables shows results from cases that are supposed to be within the limits posed by Baumann and Rehme.

Table 7.2: Calculation Results Reference Cases

Case	R_0	$R_{k1,k2}$	$R_{0_{k1,k2}}$	R	f
Baumann & Rehme (P)	7.1	3.12	2.9	7.63	0.127
Enlarged Diameter (Q)	4.2	2.95	2.9	4.22	0.098

7.2 Nikuradse

In the table below the results for the friction factor by use of Nikuradse's method are found. All of the cases, except the Smooth Pipe, are considered to be in the fully rough regime, and are assigned the value $B = 8$. The results seems logical by inspection. Worth noting can be the result of Nikuradse's friction factor for Baumann and Rehme's case. The friction factor is not significantly different than the one calculated by Baumann and Rehme's method.

Table 7.3: Calculation Results Nikarudse Roughness

Case	B	k [mm]	r [mm]	f
G	8	5.5	18	0.154
I	8	2.5	18	0.095
Enlarged Diamter (Q)	8	5.5	170	0.049
Baumann & Rehme (P)	8	10	50	0.117
Smooth Pipe (O)	5	~ 0	18	0.007

A limitation of Nikuradse's method might be that it only evaluates the roughness height in relation with the radius of the pipe. Effects belonging to the roughness

environment, that is the shape of the deposits, is lost. That is why cases K and M are not included here, since they will prevail an identical results as cases G and I for corresponding roughness heights.

7.3 Simulations

7.3.1 Wall Treatment Roughness

As mentioned earlier, the simulation in FLUENT consisted of two different types of simulations. Table 7.4 shows the results from the Wall Treatment Roughness, which is FLUENT's in-built way of treating with roughness effects. Sand Grain Roughness, rising from Nikuradse's definition, is defined when setting the parameter C_s equal to 0.5. Roughness that is a result of non-uniform spaced roughness elements are defined in the region between 0.5 and 1.

TABLE 7.4: Simulation Results Wall Treatment Roughness

Sand Grain Roughness $C_s = 0.5$		**Non-uniform Roughness** $C_s = 0.75$		$C_s = 1$	
Case	Friction Factor	Case	Friction Factor	Case	Friction Factor
A	0.071	B	0.086	C	0.104
D	0.052	E	0.060	F	0.069

Cases A, B and C are simulated with a roughness height of 5.5mm, while D, E and F shows the results for 2.5mm. The results for $C_s = 0.5$ shows somewhat lower values than achieved by the Nikuradse calculation. The reason for this might lie in the determination of the roughness function B in Nikuradse's method, or in some of the input parameters used in the simulations.

7.3.2 Cavity Induced Roughness

Table 7.5 and 7.6 show the results obtained after simulating a geometry of rectangular- and rippled roughness. As both of these cases in theory can be seen upon as uniform, though maybe not in the same degree as sand grain roughness, the results here show higher values than those obtained by the Wall Treatment Simulations. This is especially true for the case of rippled roughness.

However, as there is very little information put forward by ANSYS FLUENT regarding the definition of the C_s factor it is difficult to draw to many conclusion regarding which type of geometry it could be compared to. That being said, results from case G and I are quite close to the corresponding values for cases C and F ($C_s = 1$). Case K is identical to the corresponding case B ($C_s = 0.75$).

TABLE 7.5: Simulation Results Cavity Induced Roughness

Rectangular Roughness		**Rippled Roughness**	
Case	Friction Factor	Case	Friction Factor
G	0.153	H	0.267
I	0.067	J	0.078
K	0.086	L	0.264
M	0.072	N	0.090

If one assumes that the table above displays a correct image of the friction factor for rectangular and rippled roughness respectively, then it is clear that the effect of rippled deposits induces considerably larger friction than rectangular deposits. What is worth noting is that the leap from G to K is not proportional to the leap from H to L. Case G and H displays a roughness height of 5.5mm and a pitch equal to 56mm, while case K and L are simulated with $h = 5.5$ and $p = 35$.

By looking at Figure 7.1 which portrays rippled and rectangular roughness respectively, one might try to understand why the difference between G and K are so different from the distance between H and L. Since the distance between the rough elements, and the height of them, are the same it could be reasonable to assign the

difference to down flow effects occurring after passing the rough elements. It definetly seems like the effect of closer placed roughness elements significantly reduces the friction factor for rectangular roughness while it only slightly drops for rippled roughness.

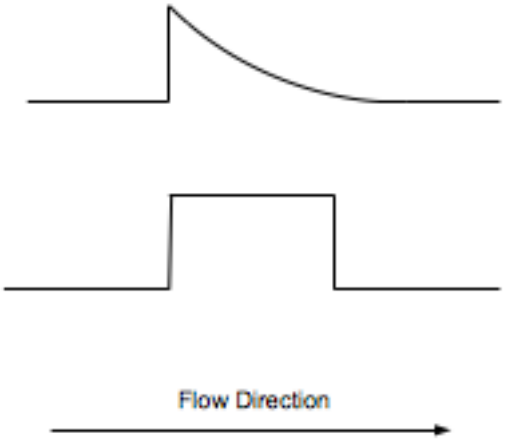

FIGURE 7.1: Constructed Geometry

All the results obtained by simulations are considerably smaller than the calculated results from Baumann and Rehme. Even the simulated result for the Baumann & Rehme case deviates considerably from the calculated value of 0.127. There might be different reasons for this. One, the simulation model is not compatible to handle the structural dimensions. If so, it will most likely be a question about the adaptability of the mesh. The other reason might be an incompatibility of the dimensions used in combination with using the Baumann and Rehme-method, even though this is not evident from the defining limits.

TABLE 7.6: Simulation Results Reference Cases (Rectangular Roughness)

	Case	**Friction Factor**
Smooth Pipe	O	0.014
Baumann & Rehme	P	0.063
Enlarged Diameter	Q	0.031

The closest results between simulated and the calculated values, are found between the rectangular roughness cases and corresponding values calculated by Nikuradse.

8. Discussion

Chapter 8 will compare and discuss the results obtained in connection with this master thesis. Results will be commented and explained in light of what has been presented previously in this study.

8.1 Comparing Results

The comparison of results will mostly consist of presenting graphs that shows how compatible results obtained from simulations are to Baumann & Rehme or Nikuradse, respectively.

8.1.1 Rectangular vs. Wall Treated Simulation

Figures 8.1 to 8.3 compare results obtained by simulating the rectangular geometry. The three graphs show all relevant cases for $C_s = 0.5$, $C_s = 0.75$ and $C_s = 1$, respectively. By observing these graphs, it is clear that Case G shows the biggest deviation between the two types of simulations. Further, it seems that the results become more alike when the roughness function C_s is increased. This might be an indication that rectangular roughness can be considered as highly non-uniform, by the definition posed by FLUENT.

In chapter 6 findings regarding the size of the friction factor was presented. There it was reported that a friction factor resulting from rectangular roughness was seven times bigger than that of sand grain roughness (Webb and Kim 2005). Here, the rectangular roughness shows at its maximum a deviation of two times higher results than the wall treated roughness. It is reasonable to compare these as rectangular versus sand grain roughness, since FLUENT uses Nikuradse's sand grain analysis.

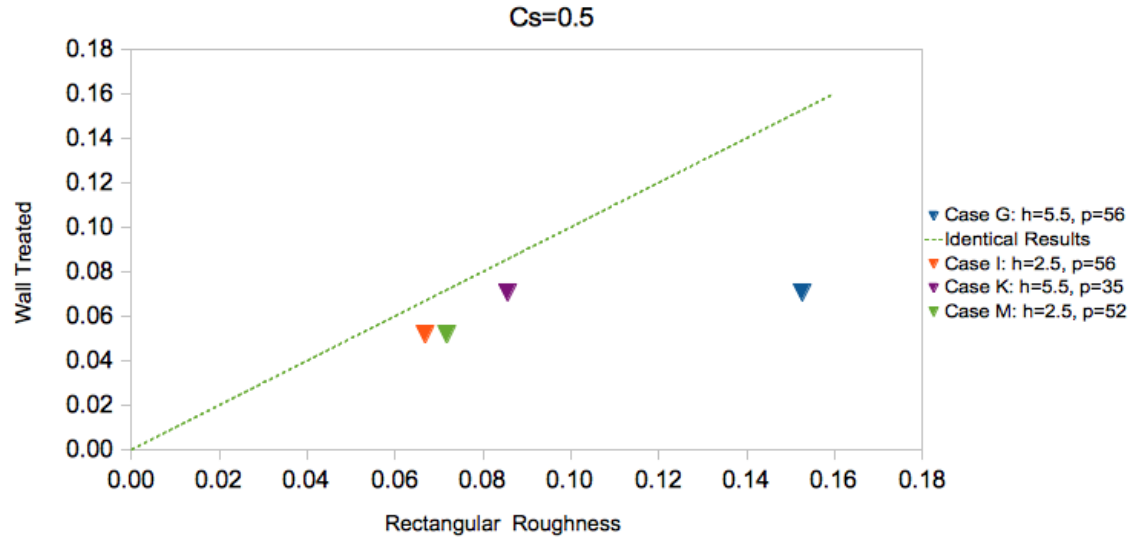

FIGURE 8.1: Rectangular vs. Wall Treated Roughness, $C_s = 0.5$

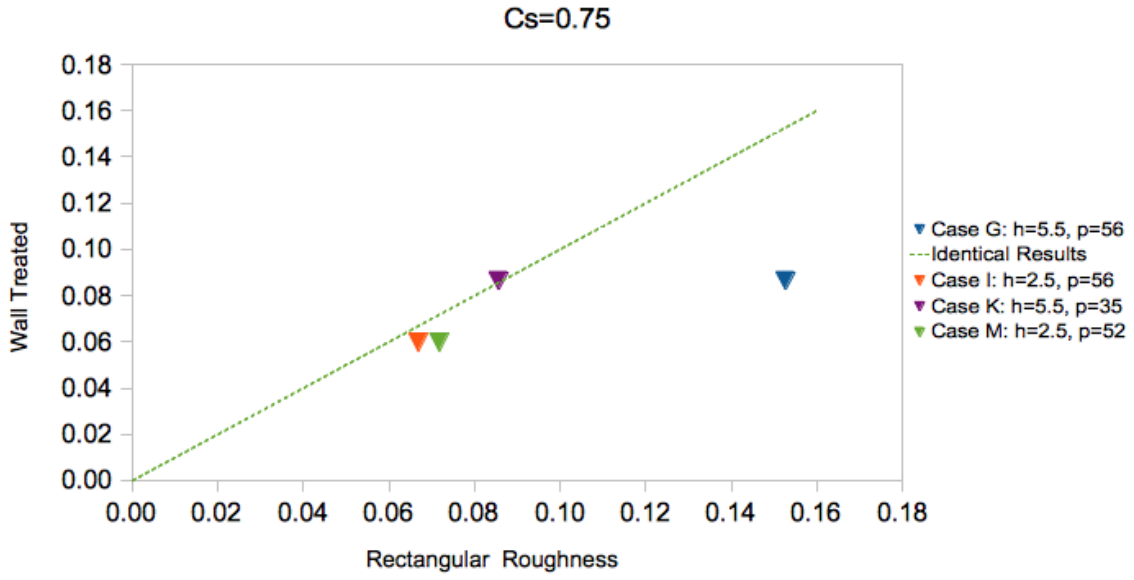

FIGURE 8.2: Rectangular vs. Wall Treated Roughness, $C_s = 0.75$

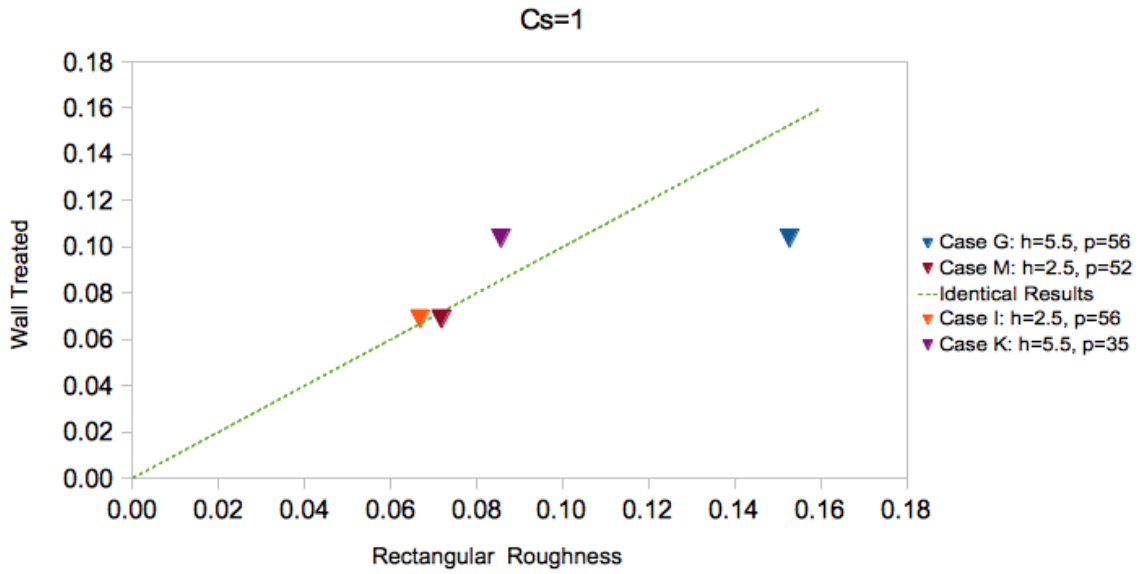

FIGURE 8.3: Rectangular vs. Wall Treated Roughness, $C_s = 1$

For rippled deposits it was reported by Bott and Gudmundsson (1978) that the friction factor of rippled deposits was significantly bigger than that calculated by sand grain roughness (Bott and Gudmundsson 1978). The results obtained in this thesis, though not presented in figures here, shows that the friction factor at its maximum is about four times bigger than the friction factor resulting from the Wall Treated simulations.

8.1.2 Wall Treated Simulations vs. Nikuradse Calculations

The results presented in this section is put forward in two ways. Namely, figure 8.4 to 8.6 that show the closeness of results with respect to $C_s = 0.5$, $C_s = 0.75$ and $C_s = 1$, respectively. While figures 8.7 and 8.8 show a comparison with respect to $k_s = 5.5mm$ and $k_s = 2.5mm$, respectively.

Figure 8.4 to 8.6 show that results simulated by FLUENT, using the near wall treatment, is closest to the calculated values of Nikuradse when the roughness height is smaller.

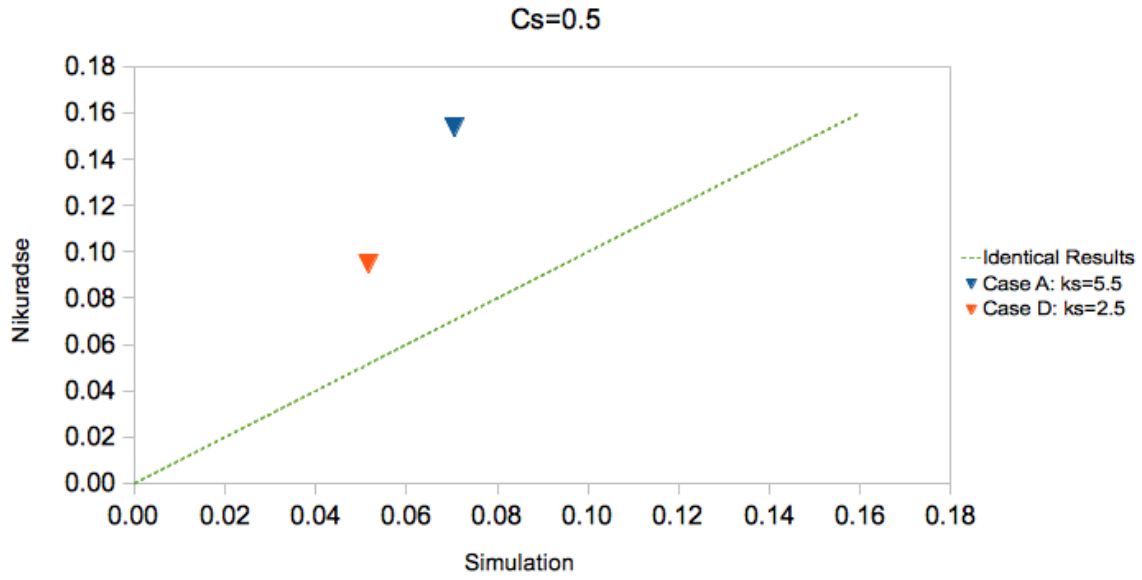

FIGURE 8.4: Wall Treated Roughness, $C_s = 0.5$, vs. Nikuradse

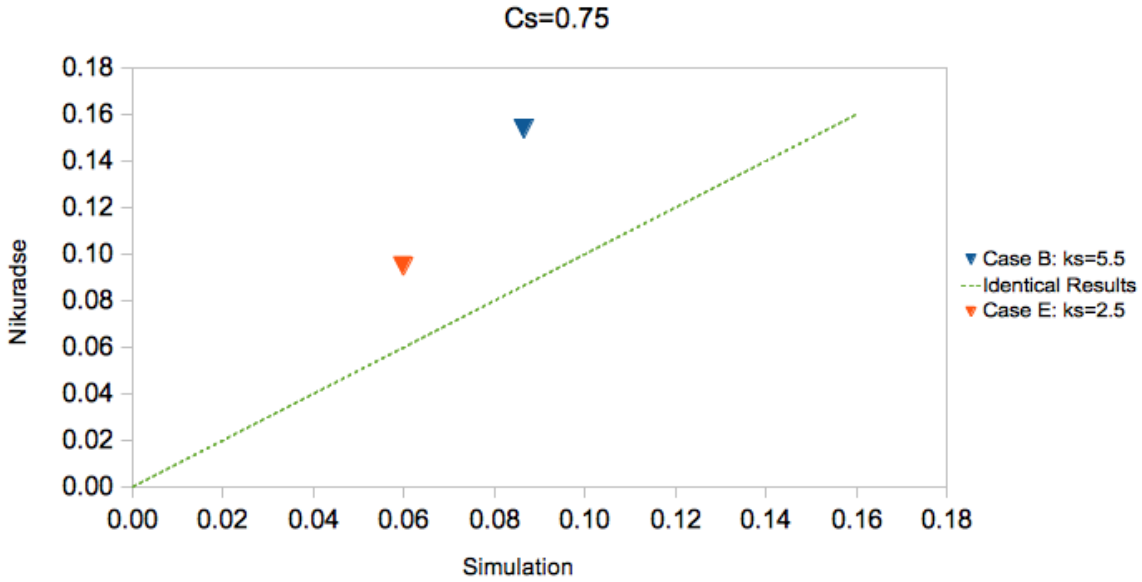

FIGURE 8.5: Wall Treated Roughness, $C_s = 0.75$, vs. Nikuradse

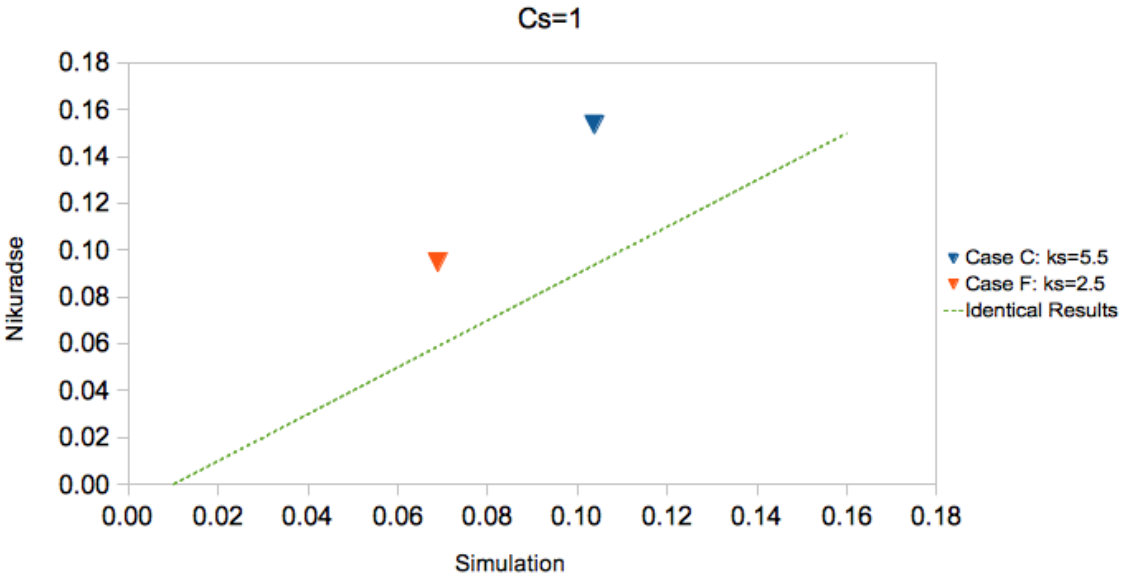

FIGURE 8.6: Wall Treated Roughness, $C_s = 1$, vs. Nikuradse

The two graphs, 8.7 and 8.8, show that, contrary to what would be expected, it is actually simulations run with $C_s = 1$ that gives the best match with Nikuradse's values. As Nikuradse, by definition, calculates the friction factor based on the analysis on equivalent sand grain roughness, it would be reasonable to expect that the simulations run with $C_s = 0.5$ would be best matched. FLUENT states that a C_s factor equal to 0.5 is equivalent to sand grain roughness as it is defined by Nikuradse (ANSYS Inc 2009a). The reason for this deviation might be a result of the somewhat dubious k/R ratio used in most of the simulations run.

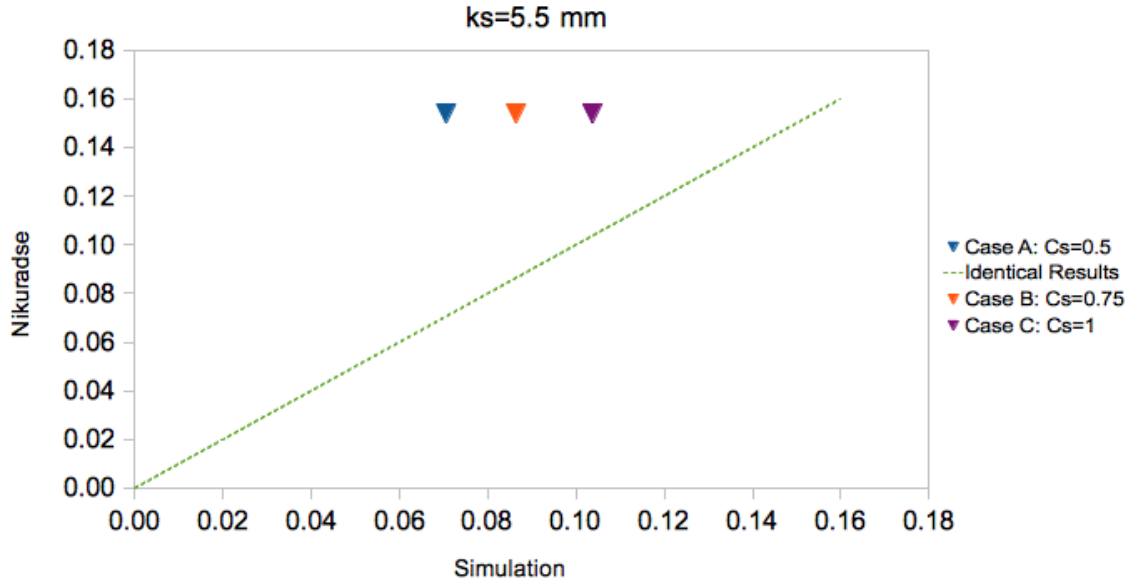

FIGURE 8.7: Wall Treated Roughness, $k_s = 5.5mm$, vs. Nikuradse

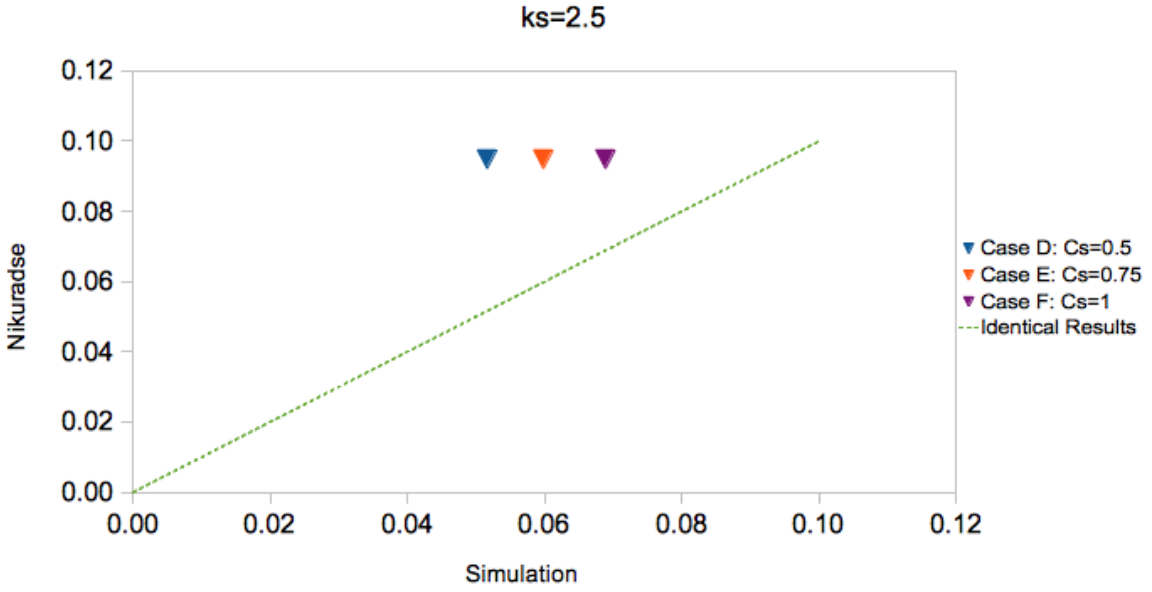

FIGURE 8.8: Wall Treated Roughness, $k_s = 2.5mm$, vs. Nikuradse

8.1.3 Rectangular Simulation vs. Baumann & Rehme Calculations

Figure 8.9 portrays the match between simulated rectangular roughness and calculated rectangular roughness, by use of Baumann & Rehme's method.

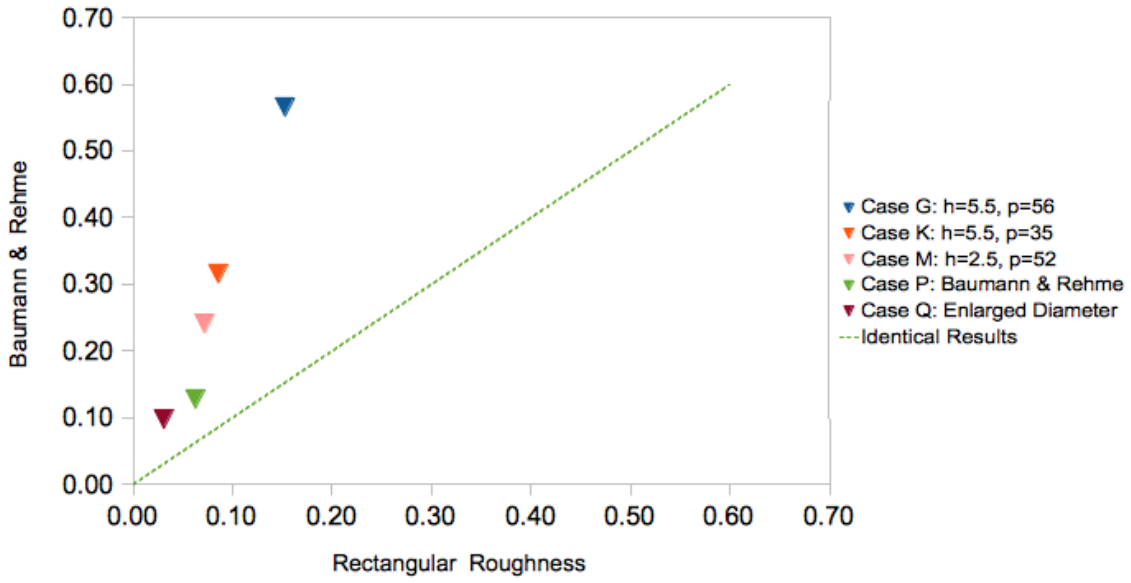

FIGURE 8.9: Simulation of Rectangular Roughness vs. Baumann & Rehme

It can be observed that this is not an ideal match, even though it should be. The simulated geometry is constructed after Baumann & Rehme's principles, and are all within the presented limits. However, what is very interesting to note is that the closest results are obtained for Cases Q, P and M, respectively. These cases are either run with a larger diameter (Case Q and P) or has a smaller roughness height (Case M). It has unfortunately not succeeded the author of this report to find any limits on the h/L ratio, that is, the relation between the roughness height and the radius for flow through a circular pipe. These results might be an indication that there actually are limitations to this relationship. However, bear in mind that the deviation for Cases Q, P and M are still not insignificant, though it might seem so. The scaling of the graph might lead to falsely thinking that the results are closer than they actually are. Also, the strongest indication that the models are not totally

compatible, is the fact that the simulated Baumann & Rehme case are only half of the calculated value.

8.1.4 Rectangular Simulations vs. Nikuradse Calculations

Figure 8.10 gives the comparision between rectangular roughness and calculated values using Nikuradse's formula.

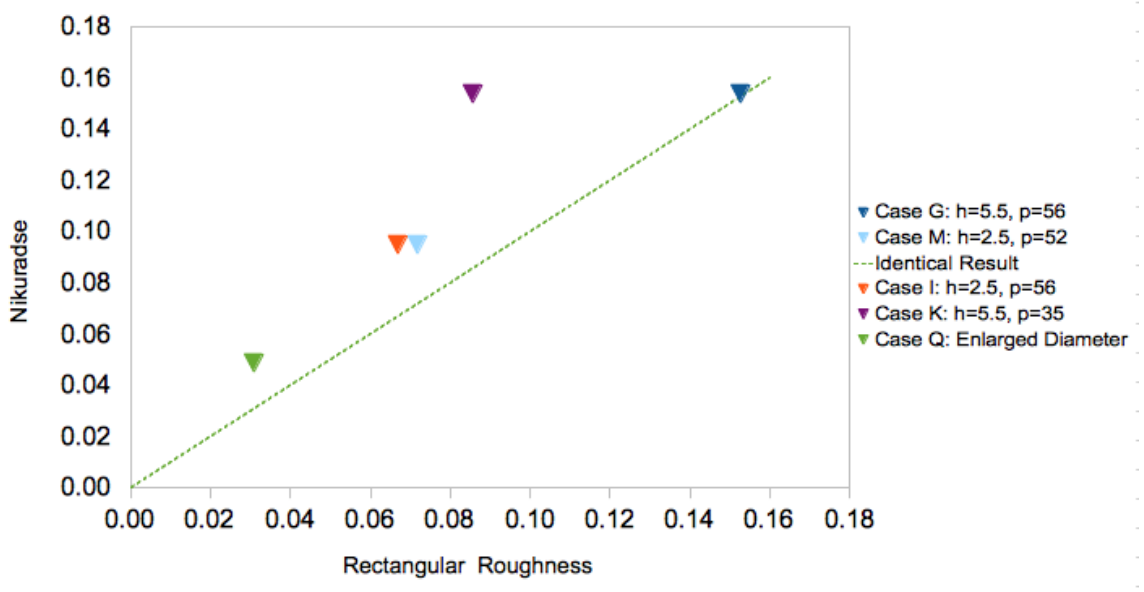

FIGURE 8.10: Simulation of Rectangular Roughness vs. Nikuradse

Compared to the Baumann & Rehme case, these values are much closer to each other. All of the plotted cases are quite close to the calculated values, except for Case K. Case K was run with a smaller pitch than corresponding Case G, which seems to have an effect. The friction factor resulting from simulating with a smaller pitch gave in this case, a smaller friction factor. If this is due to physical effects, such as the behavior of eddies, or if it is a result of an inadequate mesh, is hard to say.

8.1.5 Rippled Simulations vs. Baumann & Rehme Calculations

Figure 8.11 plots the results of the rippled simulation in relation to values obtained by Baumann & Rehme's method. Case J is not included here, since it falls outside the limits posed by Baumann & Rehme. As previously mentioned in the result section, rippled simulations came out with marked higher friction factors compared to results from rectangular simulations. By assuming that Baumann & Rehme's method can be used for rippled deposits too, one can see that the results are generally closer to the calculated values in the case of a rippled deposit.

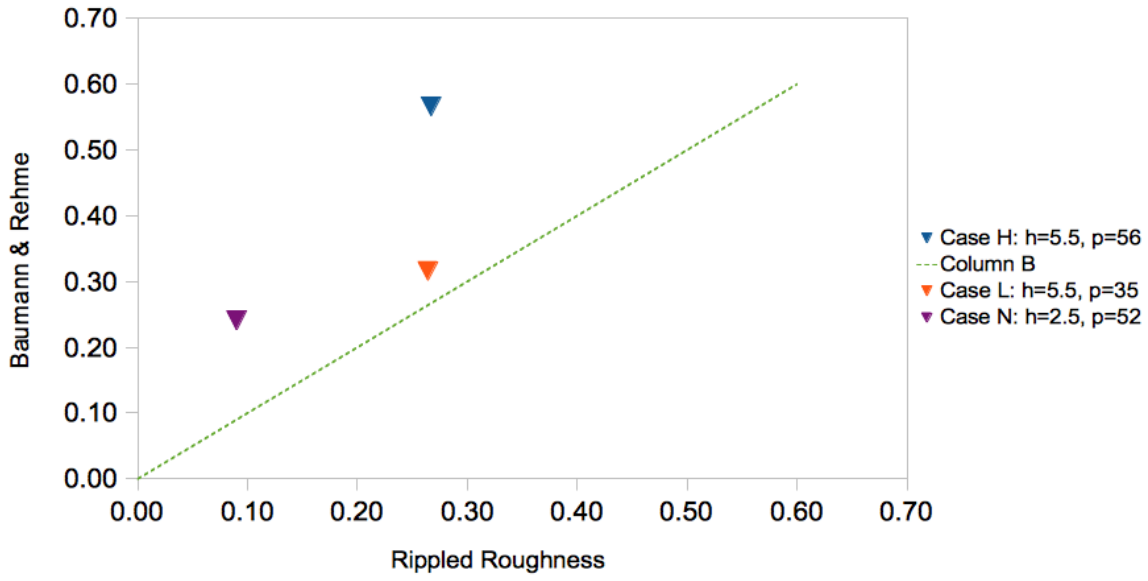

FIGURE 8.11: Simulation of Rippled Roughness vs. Baumann & Rehme

Here, Case L are found to give the best matched case, while Case N are more or less as closely matched as in the case of rectangular roughness. However, the simulated friction factor for Case L are questionably high compared to the corresponding results in rectangular roughness. So, then it is a question of whether the rippled or the rectangular simulation gives the most appropriate answer. Again, be aware of the coarse scaling of the graph possibly leading to falsely believing that the results are a closer match then they really are.

8.1.6 Rippled Simulations vs. Nikuradse Calculations

First, by observing Figure 8.12, which represents the rippled simulations against the values from corresponding cases calculated by Nikuradse, one can see that the results of each roughness height is very close. This is a sign that shows that Nikuradse do not include the geometry of the given roughness deposit. The previous presented graph, 8.11, showed a scatter, both vertically and horizontally, due to the inclusion of both height, pitch and width.

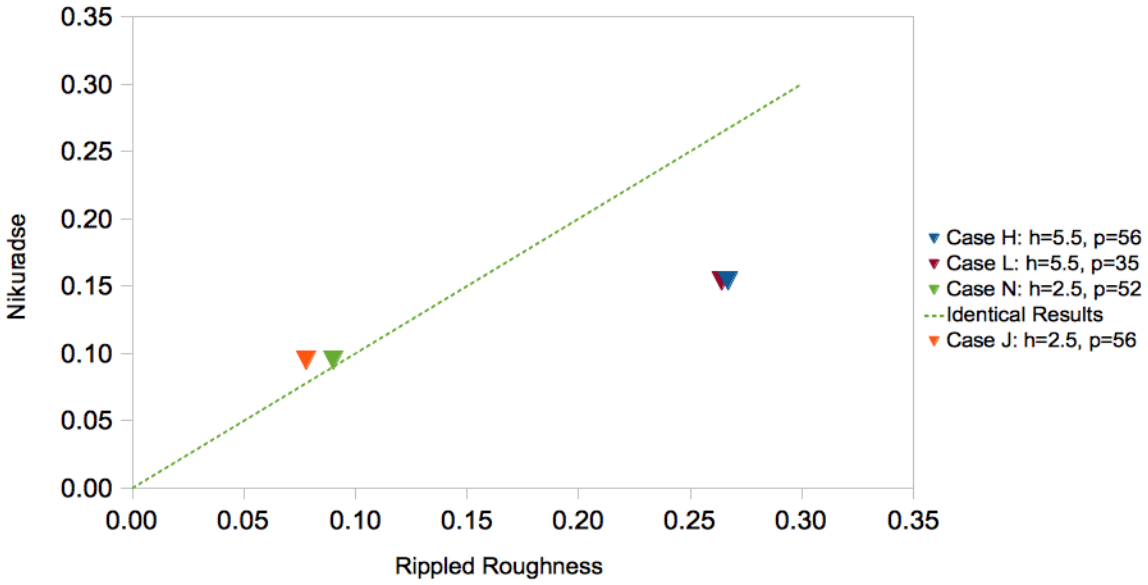

FIGURE 8.12: Simulation of Rippled Roughness vs. Nikuradse

Clearly, from observing graph 8.12, Case N and J are the best matches to Nikuradse. However, Case L is questionably high compared to its corresponding rectangular case, Case K. It is important to note that Case N and J, actually are quite close to Nikuradse, because the scaling of graph 8.12 is much smaller than of the graph 8.11.

8.1.7 Rectangular vs. Rippled Simulations

The last results to be compared are rectangular against rippled deposits. Figure 8.13 show the four corresponding cases matched against each other. The takeaway

from this is that the Case M vs. N and Case I vs. J, which are the simulations run with the smallest roughness heights, are extremely well matched. However, one can still see that results obtained by the rippled simulations are a tad higher. This is to be expected, as rippled deposits have been said to give higher friction factors in previously published papers (Gudmundsson 2010).

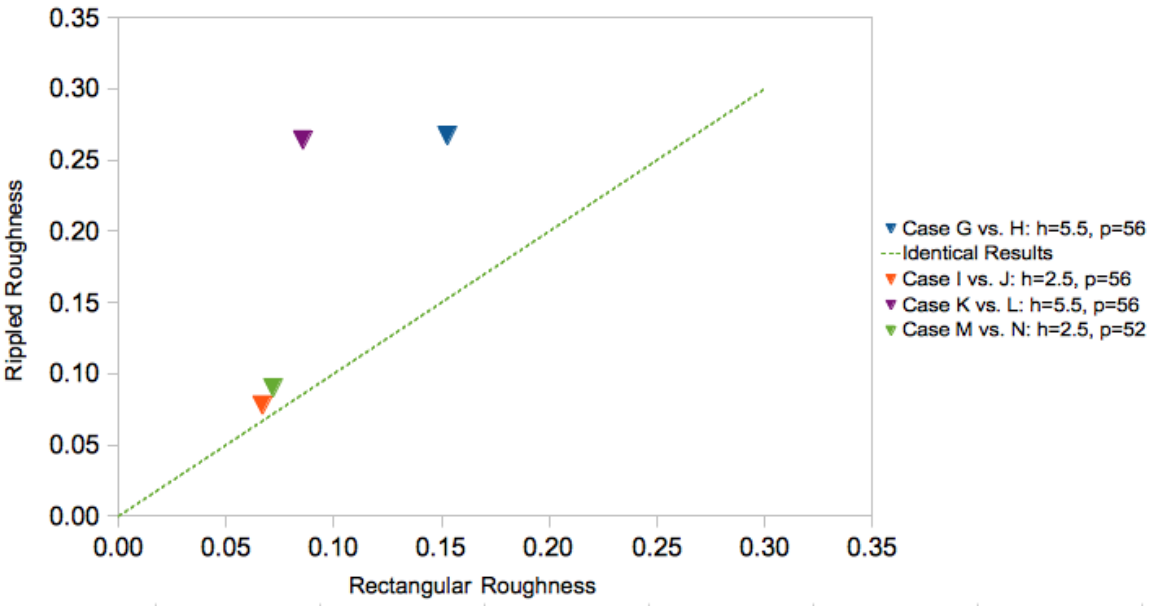

FIGURE 8.13: Rectangular vs. Rippled Roughness

Actually, it is more interesting to discuss why these cases are so similar. It might be because the simulation in FLUENT does not "detect" the difference in shape when the roughness elements are getting smaller and the distance between them are fairly big. This would be linked to the construction of the mesh, and could probably be improved by a more experienced user of FLUENT. Another explanation could be that the results are as to be expected, and that the difference between rippled and rectangular roughness increases as the height of the roughness elements increases.

Between Case G vs. H and K vs. L the deviations are bigger. This is especially true for Case K vs. L, but again, the value of either K or L are unlikely to be accurate. In the Case of G vs. H, the friction factor obtained by the rippled simulation are about the double of the rectangular result. While Case L (rippled) are about four times bigger than Case K (rectangular).

8.1.8 Summing Up

- Rectangular simulations are fairly well matched to results obtained by Wall Treaded simulations, except from the case G (h=5.5, p=56). The results are matching more as the C_s factor increases.
- Wall Treated Roughness and Nikuradse are found be closest when $C_s = 1$ and for the smallest roughness height, $k_s = 2.5$.
- Friction factors calculated by Baumann & Rehme are significantly higher than the values obtained by the rectangular simulations. This might be an indication that Baumann & Rehme is not valid for the simulated h/L dimensions.
- Rectangular roughness seems to be fairly well matched by Nikuradse.
- The simulation of rippled roughness is closer to Baumann & Rehme, though it can not be said that it is a very close match.
- Results from rippled simulations are a fair match to Nikuradse for smaller roughness heights, though not a very good match for the cases run with $k_s = 5.5mm$.
- Lastly, information gained by comparing rippled against rectangular simulations shows that rippled roughness indeed give higher friction factor. It also, seems that this trend increases along with increased roughness heights.

8.1.9 Diameter Adjustments

Before concluding this analysis, it would be interesting to see if there is any changes in the takeaways, if the diameter used to calculate the friction factor is defined differently. The previous presented results are by use of a diameter defined to be the outer surface's diameter. Other possibilities are, for example, the inner diameter (between the top of the rough elements) or an intermediate diameter (the distance between half of the roughness elemens). Table 8.1 shows the results of such adjustments.

Table 8.1: Diameter Adjusted Results

Case	Outer Diameter	Mid Diameter	Inner Diameter
G	0.153	0.129	0.106
I	0.067	0.062	0.058
K	0.086	0.073	0.059
M	0.072	0.067	0.062

As can be seen in table 8.1, the results move towards smaller values of the friction factor as the diameter decreases. This is a logical result when interpreting Darcy's friction factor relationship, however, it increases the deviation between the simulated results and Baumann & Rehme's. As the diameter decreases, the friction factor increases when using Baumann & Rehme's method.

8.2 Discussion of Results

In this report, the aim has been to establish whether FLUENT can be used as a software to model roughness or not. In order to evaluate the results obtained by the simulations, the results have been compared to a few proposed methods to calculate the friction factor in rough regimes, presented in previous literature. After finishing simulations on rectangular, rippled and sand grain roughness the author of this report can not say that it has been a success without limitations.

8.2.1 Baumann & Rehme

Comparing results obtained by simulating rectangular roughness to Baumann & Rehme clearly shows significantly lower results of the friction factors for the simulations. This might be linked to either one of these two reasons;

1. The friction factor obtained by using Baumann & Rehme yields unnaturally high friction factors. This can either be due to a fault in the interpretation

of this method, or possibly, an undiscovered limitation of the relationship, h/L, that is the roughness size compared to the radius of the pipe. The cases presented in this report does have a somewhat disproportional relationship between the roughness size and the dimensions of the pipe.

2. Secondly, the simulation might be subject to a poor mesh or being affected by the disproportional relationship presented above.

To draw any finite conclusions here, is challenging. However, since the simulated result of Case P, which is an example presented by Baumann & Rehme, yields a friction factor around half the one calculated by Baumann & Rehme, it seems in this case that the simulation presents the errors. Yet again, this might be difficult to say for sure. Baumann & Rehme used a set of experiments conducted by a various of authors when they developed their method. It is difficult to say how they determined the velocity used when calculating the friction factor. Did they measure the inlet and outlet velocity, and deduced a mean? In the simulations the velocity was read from a stable rough section, and the pressure drop was taken from the same interval. Also, if there really is no limitation on the h/L relationship, then the calculated values by Baumann & Rehme can be considered somewhat unrealistic.

8.2.2 Sand Grain Roughness

Rectangular roughness was stated to yield around seven times higher friction factor than obtained by sand grain roughness. The simulation of sand grain roughness does yield smaller friction factors than the ones obtained by rectangular roughness, though not to the extent referred to by Webb and Kim (2005). The deviation between these two simulated results seem to increase with increased roughness heights. Case K, as previously pointed out, shows a suspicious low result. This might in fact be due to the shorter distance between the rough elements. By information presented by Webb and Kim (2005) it might be that reattachment of the flow never occurs, and this might very well affect the result obtained by this simulation. The

corresponding case for rippled roughness yields a much larger friction factor, which is the expected result. The flow across a rippled surface might not pose the same limitations, or behavior, as flow across rectangular rough elements.

The simulated sand grain roughness does not present identical results to the calculated sand grain roughness, which would be an ideal result. The calculated values are larger than the simulated friction factors. However, this might be connected to the roughness factor, B, used. In the calculation $B = 8$ is used for a fully rough regime, while FLUENT calculates this value by use of the formula presented below:

$$\Delta B = \frac{1}{\kappa} ln(1 + C_s K_s^+) \tag{8.1}$$

κ is Van Karmen's constant, C_s is the roughness constant previously explained and K_s^+ is the characteristic dimensionless roughness height. When using the same K_s^+ that was found when establishing which regime the situations belonged to, ΔB yields somewhat higher values than $B = 8$. By increasing B the friction factor will be decreased, which can explain why the simulated and calculated results are not identical.

8.2.3 Rectangular vs. Rippled Roughness

Previous observations have suggested that the resulting friction factor from rippled deposits is larger than the one obtained by rectangular deposits. This seems to be confirmed by the simulations conducted in this thesis.

9. Conclusions

- Sand Grain Roughness are well modeled by the simulations when the roughness function, B used to calculate Nikuradse's friction factor, is adjusted to resemble the one used in the simulations.

- Rippled roughness, for the highest roughness height, give around twice as high friction factor compared to rectangular roughness, while rectangular roughness yields a twice as high result than simulated sand grain roughness.

- The simulation of Baumann & Rehme's Case yields a considerably lower friction factor than the calculation does for the same case. This might be a result of an unexplained limitation on the relation between the roughness height and the radius of a pipe.

- Flow characteristic across a rough element, or poor quality of mesh in FLUENT, can be possible sources of uncertainties. This results from limited knowledge regarding both of these areas.

10. Further Work

- More knowledge around meshing is needed to assure quality results in FLUENT. Also, an advantage would be to learn how to use GAMBIT, which is a program that FLUENT can use to create the geometry involved. It is a separate program, but might help to make the construction process somewhat easier.

- The roughness analysis should be linked to heat transfer theory, and this should be included in the simulations run in FLUENT. In order to this, a better construction of the cavity constructed geometry needs to be established. Creating a compact outer surface, with only rough elements protruding inwards was not succeeded in this analysis.

- More knowledge on the flow characteristic across rough elements, and its influence on the resulting friction factor would be beneficial in a future report.

References

ANSYS Inc (2009a). *ANSYS FLUENT 12.0 Theory Guide*. ANSYS Inc.

ANSYS Inc (2009b). *ANSYS FLUENT 12.0 Tutorial Guide*. ANSYS Inc.

ANSYS Inc (2009c). *ANSYS FLUENT 12.0 User Guide*. ANSYS Inc.

Arasu, A. V., Sasmito, A. P., and Mujumdar, A. S. (2011). Numerical performance study of paraffin wax dispersed with alumnia in a concentric pipe latent heat storage system. *Department of Mechanical Engineering Thiagarajar College of Engineering and Department of Mechanical Engineering National University of Singapore*.

Baumann, W. and Rehme, K. (1974). Friction correlations for rectangular roughnesses. *Pergamon Press*, 18:1189–1197.

Bern, P., Withers, V., Cairns, R., and BP (1980). Wax deposition in crude oil pipelines. *European Offshore Petroleum Conference*.

Botne, K. (2011). Modeling wax deposition with deposition-release models. Specialization project-ntnu, NTNU.

Botne, K. (2012). Modeling of wax thickness in single-phase turbulent flow. Master's thesis, Norwegian University of Technology and Science, NTNU.

Bott, T. (1997). Aspect of crystallization fouling. *School of Chemical Engineering, University of Birmingham, Elsevier Science Inc.*

Bott, T. and Gudmundsson, J. S. (1978). Rippled silica deposits in heat exchanger tubes. *International Heat Transfer Conference, Hemisphere Publishing Corporation.*

Donne, M. D. and Meyer, L. (1977). Turbulent convective heat transfer from rough surfaces with two-dimensional rectangular ribs. *Pergamon Press*, 20:583–620.

Edmonds, B., T.Moorwood, Szczepanski, R., and Zhang, X. (2008). Simulating wax deposition in pipelines for flow assurance. *Energy Fuels*.

Elsharkawy, A., Al-Sahhaf, T., and Fahim, M. (1999). Wax deposition from middle east crudes. *Petroleum and Chemical Engineering Department, University of Kuwait*.

Fong, N. and Mehrotra, A. K. (2007). Deposition under turbulent flow of wax-solvent mixtures in a bench-scale flow-loop apparatur with heat transfer. *Energy and Fuels, Department of Chemical and Petroleum Engineering University of Calgary*, pages 1263–1276.

Gudmundsson, J. (1981). *Particualte Fouling, Fouling of Heat Surfaces*. Hemisphere Publishing Corporation.

Gudmundsson, J. (2009). *Kompendium TPG 4135, Prosessering av Petroleum, Grunnleggende enhetsoperasjoner i produksjon av olje og gass*. Department of Petroleum Engineering and Applied Geophysics, NTNU, Trondheim.

Gudmundsson, J. (2010). *Flow Assurance, Solids in Oil and Gas Production (First Draft)*. Department of Petroleum Engineering and Applied Geophysics, NTNU, Trondheim.

Guha, A. (2008). Transport and deposition of particles in turbulent and laminar flow. *Aerospace Engineering Department, University of Bristol, UK*.

Handal, A. (2008). Analysis of some wax deposition experiments in a crude oil carrying pipe. Master's thesis, Master Thesis-University of Oslo.

Hoffmann, R. and Amundsen, L. (2009). Single-phase wax deposition experiments. *Energy Fuels*.

Huang, Z. (2011). *Application of the Fundamentals of Heat and Mass Transfer to the Investigation of Wax Deposition in Subsea Pipelines*. PhD thesis, University of Michigan.

Kane, M., Djabourov, M., and Volle, J.-L. (2004). Rheology and structure of waxy crude oils in quiescent and under shearing conditions. *FUEL*, 83.

Kjøraas, M. (2012). Modeling of wax deposition along subsea pipelines. Technical report, Department of Petroleum Engineering and Applied Geophysics, NTNU.

Lu, Y., Huang, Z., Hoffman, R., Amundsen, L., and Fogler, H. (2012). Counterintuitive effects of the oil flow rate on wax deposition. *Energy and Fuels*.

Marshall, G. (1988). Cleaning of valhall offshore oil pipeline. *Offshore Technology Conference, OTC*.

Maubach, K. (1970). Reibungsgesetze turbulenter strornungen*. *Gesellschaft fur Kernforschung mbH, Karlsruhe*.

Moran, M. J. and Shapiro, H. N. (2007). *Fundamentals of Engineering Thermodynamics*. John Wiley and Sons, Inc, 5 edition.

Parthasarathi, P. and Mehrotra, A. K. (2005). Solids deposition from multicomponent wax-solvent mixtures in a benchscale flow-loop apparatus with heat transfer. *Department of Chemical Engineering, University of Calgary, Canada*.

Rønningsen, H. P. (2012). Production of waxy oils on the norwegian continental shelf: Experiences, challanges, and practices. *Energy and Fuels*.

Rosvold, K. (2008). Wax deposition models. *Master Thesis- NTNU*.

Siljuberg, M. (2011). Shear dispersion of particles in pipe flow. Technical report, Department of Petroleum Engineering and Applied Geophysics, NTNU.

Siljuberg, M. (2012). Modeling of paraffin wax in oil pipelines. Master thesis, Department of Geophysics and Petroleum, Norwegian University of Technology and Science.

Singh, A., Lee, H., Singh, P., and Sarica, C. (2011). Ss: Flow assurance: Validation of wax deposition models using field data from a subsea pipeline. *Offshore Technology Conference, OTC*.

Singh, P., Fogler, H., and Nagarajan, N. (1999). Prediction of the wax content of the incipient wax-oil gel in a pipeline: An application of the controlled-stress rheometer. *The Society of Rheology, Inc.*

Singh, P., Venkatesan, R., Fogler, H., and Nagarajan, N. (2001). Morphological evolution of thick wax deposits during aging. *AIChE Journal*, 47.

Su, Z. (1996). *Pressure Drop in Perforated Pipes for Horizontal Wells*. PhD thesis, Norwegian University of Science and Technology, Department of Petroleum Engineering and Applied Geophysics.

Toor, H. and Marchello, J. (1958). Film-penetration model for mass and heat transfer. *Carnegie Institute of Technology, Pittsburgh, Pennsylvania*.

Venkatesan, R., Fogler, H., Nagarajan, N., and Singh, P. (2000). Formation and aging of incipient thin film wax-oil gels. *Dept. of Chemical Engineering, University of Michigan*, 46(5).

Webb, R. L. and Kim, N.-H. (2005). *Principles of Enhanced Heat Transfer*. Taylor and Francis Group.

A. FLUENT

A.1 Images

All results and procedures is included in previous chapters. In this section, some images are presented in order to show both the geometry, and possible effects the flow experiences when passing a rough element.

The color scheme in figure A.1 to A.4 signifies the velocity magnitude belonging to the water flow. Dark blue represent the no-slip criteria, that is zero velocity. Dark red is the highest velocity belonging to the given case.

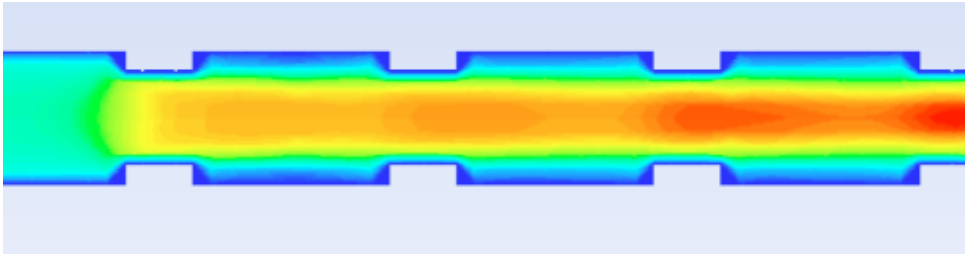

FIGURE A.1: Image of the Velocity Magnitude belonging to Rectangular Roughness

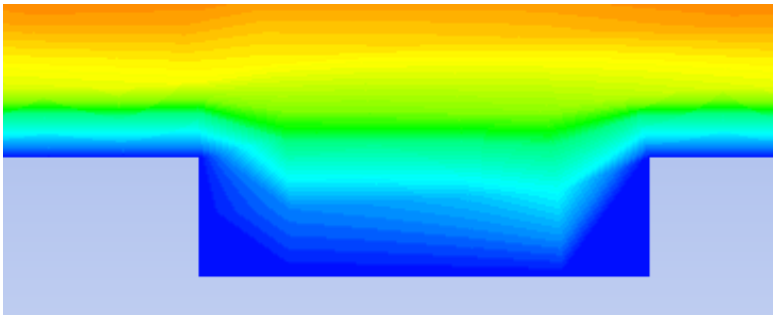

FIGURE A.2: Velocity Magnitude across a Rectangular Rough Element

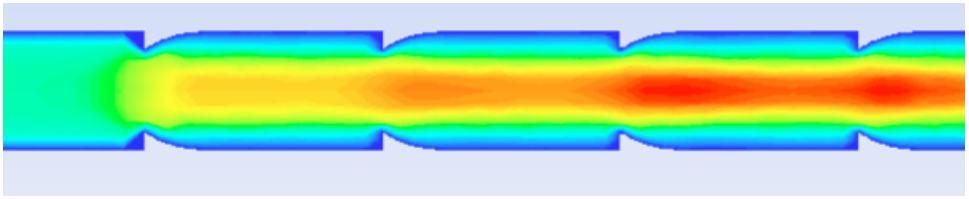

FIGURE A.3: Image of the Velocity Magnitude belonging to Rippled Roughness

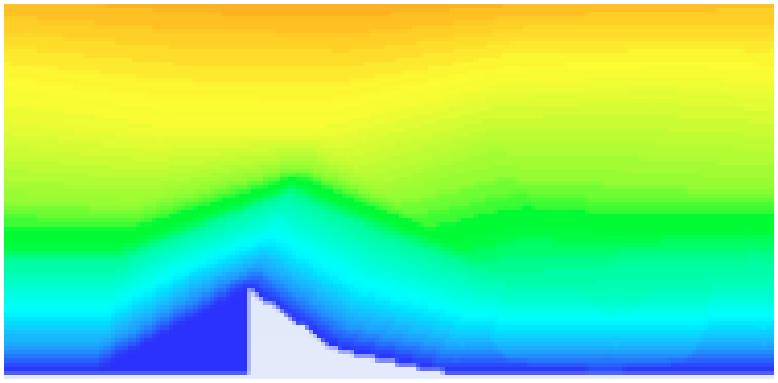

FIGURE A.4: Velocity Magnitude across a Rippled Rough Element

By comparing figure A.2 and A.4 it seems that the no-slip condition is stronger enforced for rectangular roughness than for rippled roughness. Wether this is a mesh related problem, or a result of the geometry itself is hard to say. However, it can definitely have an impact on the results. It can be observed the same no-slip condition upstreams the rippled rough element as between two rectangular rough elements.

Another observation is that the rough elements seem to impose a change of flow pattern, both immediately above, but also closer to the center of the pipe. The nature of the flow pattern change is, by observation, different for rectangular than rippled roughness. To understand why rectangular and rippled deposits results in different friction factors this phenomenon might be interesting to look further into.

A.2 Step-by-step FLUENT

1. Launch ANSYS Workbench
2. Drag Fluid Flow (FLUENT) into the blank work area
3. Mark Geometry. Choose either 2D or 3D as analysis type under Advanced Geometry Options in the right hand box. Then double-click on Geometry.
4. A pop-up window will emerge, select the desired units. After that a separate construction window will emerge.
5. Create the wanted geometry for the wanted co-ordinate system. Follow the User Guide in how to do this (ANSYS Inc 2009c). Save when done.
6. Update program in ANSYS Workbench. Launch Mesh.
7. Create mesh, follow instructions from User Guide (ANSYS Inc 2009c). Then create named selections, such as pipe wall, inlet, outlet and centerline if the problem is axisymmetric. Save, and exit.
8. Update program in ANSYS Workbench. Launch Setup. A pop-up window will emerge, set the wanted characteristics. Normally, double-precision is used. More information on this is found in both FLUENT's Theory and User Guide (ANSYS Inc 2009a,c).
9. A separate setup window will emerge. Follow the suggested procedure indicated by FLUENT (go from top to bottom) to define all relevant information. This includes; defining if the problem is axisymmetric, pressure or density-based, models, materials etc.
10. When all parameters are defined in the setup, continue down to the solution. Set solution convergence to other values than the default values posed by FLUENT if necessary. Otherwise, continue to define which surface is going to be set as reference for the calculation, usually the inlet for pipe flow. Save project.

11. Initialize project. Usually also done from inlet, remember to press initialize.

12. Run Calculation. Define how many iterations to use, this depends on the project in question.

13. After the solution has converged, go to "File" and into "Data File Quantities". Here, you define which parameters to include in the results. Save project and exit the setup window.

14. Launch Results from ANSYS Workbench, a separate window will emerge. Follow the User Guide's instructions on how to set up the results for the parameters in question. It is possible to export the results to Excel.

A.3 Future Recommendations

Due to the inexperienced user of FLUENT some simplifications might have been taken in order to reach the results presented in this report. The procedure followed is given in chapter 5. However, additional thoughts and recommendations will shortly be presented in this appendix.

In order to relieve the construction process, it might be beneficial to get access to GAMBIT. GAMBIT is a separate geometry device that FLUENT is able to read. In this report, the geometry was directly constructed in FLUENT, which was experienced to be both time consuming and limiting. It was not succeed to construct the desired pipe geometry with respect to both the outer- and inner pipe wall.

The geometry used here:

This geometry is defined such that the pipe wall follows the rough elements inwards. A better geometry would have a thick wall, with only intrusions inwards. This would allow for simulations on heat transfer. In order to link such simulations better to wax deposition, it should be further divided in two surfaces. A pipe wall with the properties belonging to the construction material relevant, and intrusions that consists of wax resembling properties.

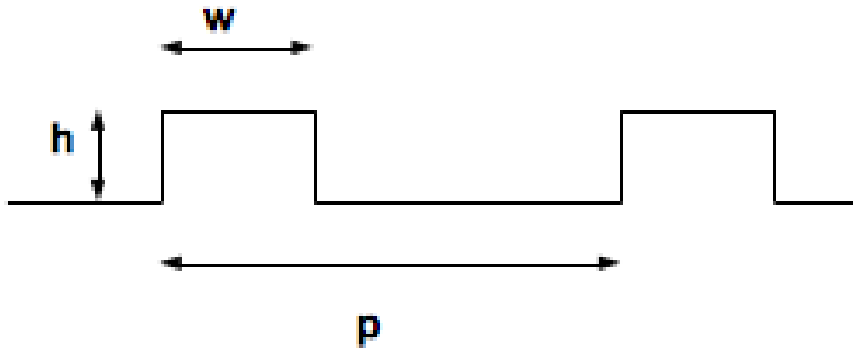

FIGURE A.5: Rectangular Geometry

An ideal geometry would look more like the figure presented in A.6:

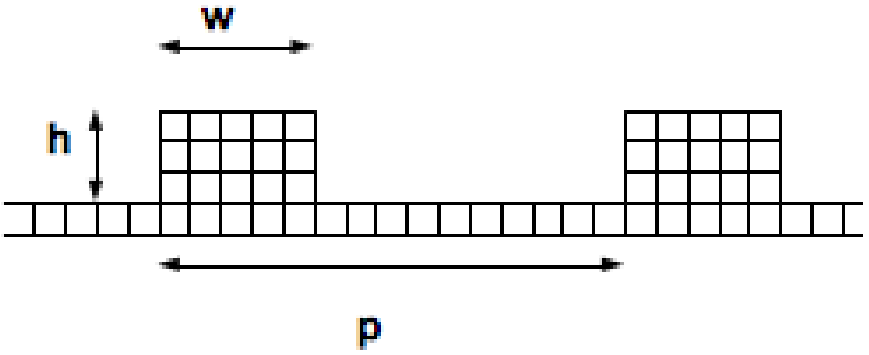

FIGURE A.6: Geometry with "filled" wall

Some suggestions on how to construct a two-layered geometry has been found on different forums related to FLUENT. One suggestion is to create a mesh for the first geometry, and then import the second geometry, however, this has not been attempted in this report. To achieve the best possible results, detailed knowledge on meshing should be acquired. This might be the most challenging part of FLUENT, and a subject to both trial and error, but the user also need to access and use knowledge on this area from FLUENT's user guide (ANSYS Inc 2009c).

In this report the fluid used was water. To simulate a wax deposition process in more general terms, not only roughness effects, a realistic crude oil or condensate fluid should be used. This might be possible to define directly into FLUENT, however,

attempts to do this has proven to be time-consuming and very manual work. A better option might be to use $C++$ language, and call this file into FLUENT.

Finally, for simulations to be worth while and to give fruitful results, considerable thought to dimensions and flow properties should be taken in advance of any simulations. Important factors to define are operating conditions, such as velocity, pressure and turbulence intensity. How to define these properties in FLUENT is explained further in FLUENT's User Guide (ANSYS Inc 2009c).

B. Overview of Cases

This appendix is included to give a complete overview over all simulations and calculations, and their respective results. The results, or how these have been reached will not be discussed here, since this have been explained or discussed previously.

B.1 Simulations

Rectangular Roughness:

TABLE B.1: Rectangular Roughness

Case	Dimensions	Radius	Friction Factor
G	$h = 5.5\ w = 14\ p = 56$	18	0.153
I	$h = 2.5\ w = 14\ p = 56$	18	0.067
K	$h = 5.5\ w = 14\ p = 35$	18	0.086
M	$h = 2.5\ w = 5\ p = 52$	18	0.072
P	$h = 10\ w = 20\ p = 40$	50	0.063
Q	$h = 5.5\ w = 14\ p = 56$	170	0.031

Rippled Roughness:

TABLE B.2: Rippled Roughness

Case	Dimensions	Radius	Friction Factor
H	$h = 5.5\ w = 14\ p = 56$	18	0.267
J	$h = 2.5\ w = 14\ p = 56$	18	0.078
L	$h = 5.5\ w = 14\ p = 35$	18	0.264
N	$h = 2.5\ w = 5\ p = 52$	18	0.090

Sand Grain Roughness:

TABLE B.3: Wall Treatment Roughness

Sand Grain Roughness $C_s = 0.5$		**Non-uniform Roughness** $C_s = 0.75$		$C_s = 1$	
Case	Friction Factor	Case	Friction Factor	Case	Friction Factor
A	0.071	B	0.086	C	0.104
D	0.052	E	0.060	F	0.069

B.2 Calculations

Baumann & Rehme:

Figure B.1 shows the calculation procedure for Case P:

	mm				
h	10		1<p/h<40	4	OK
w	20		0.3<h/w<8	0.5	OK
p	40		h/L	0.2	
L=radius	50		Ro<10	7.1	OK
G	3.75				
		1	Roughness Parameter for fictitious h/L=0		
			a1	35.67776572	
			a2	-1.26560342	
			a3	0.2977633155	
			a4	0.8180550033	
			Ro	7.1	OK
		2	Dependence of height of roughness element to the length of velocity profile		
			Rk1,k2	3.12	
		3	Constant		
			Rok1,k2	2.9	
		4	Roughness Parameter for a given h/L		
			R	7.63	
		5	Resulting friction factor		
			f	0.128	

FIGURE B.1: Calculation of Baumann & Rehme Method

TABLE B.4: Baumann & Rehme Calculation (Baumann and Rehme 1974)

Case	R_0	$R_{k1,k2}$	$R_{0_{k1,k2}}$	R	f
G	4.2	3.17	2.9	4.55	0.566
K	5.3	3.17	2.9	5.82	0.316
M	4.3	3.07	2.9	4.58	0.240
P	7.1	3.12	2.9	7.63	0.1277
Q	4.2	2.95	2.9	4.22	0.098

Nikuradse:

Table B.5: Nikarudse Roughness Calculation

Case	B	k [mm]	r [mm]	f
G/K/H/L	8	5.5	18	0.154
I/M/J/N	8	2.5	18	0.095
Q	8	5.5	170	0.049
P	8	10	50	0.117
O	5	~ 0	18	0.007

Diameter Adjusted Calculations:

Table B.6: Diameter Adjusted Results

Case	Outer Diameter	Mid Diameter	Inner Diameter
G	0.153	0.129	0.106
I	0.067	0.062	0.058
K	0.086	0.073	0.059
M	0.072	0.067	0.062

C. Heat Transfer

Appendix C was initially a part of the thesis itself, however, since the focus shifted more to solely investigate the roughness effects, it became a bit excessive. Though, it might be useful for future work if heat transfer is included, and is therefore included in the appendix.

Appendix C will present and discuss the current advantages of a heat transfer analysis to wax deposition, and it will provide some useful insight from the literature on the topic. Heat transfer will not be modeled in any simulations run in this report. However, a glance at theory seemed appropriate, and it is an area suitable for simulations in FLUENT by use of the Enthalpy-Porosity Method (ANSYS Inc 2009a).

C.1 Defining Parameters

By evaluating the heat transfer acting on a deposition regime, an analysis of energy is performed. Heat transfer is described by two main domains, namely temperature, which states the amount of thermal energy present, and flow of heat which represent the movement of thermal energy from a high state to a low. The thermal energy is an microscopic energy process, which can be referred to as an internal energy process. For thermal energy there are two terms that describes the energy processes involved. Sensible energy refers to the kinetic energy that comes from interactions between the molecules, that is vibrations, lateral movements and rotations. Further, intermolecular forces act between the molecules, that in cases when sufficient energy is supplied, or removed, induces a phase change. The energy linked to this is termed latent energy (Moran and Shapiro 2007).

C.1.1 Conduction

Conduction is one out of three ways that energy can be transported by heat, and it can take place in solids, liquid and gas. The process is related to high energetic particles transmitting energy to adjacent particles containing less energy. Conduction can be further quantified by use of Fourier's law, given below:

$$\dot{Q}_x = -\kappa A \frac{dT}{dx} \tag{C.1}$$

Where $\dot{Q}_x$ is the heat transfer, here in the x direction, κ is the thermal conductivity and $\frac{dT}{dx}$ is the temperature gradient in the x direction. The minus sign is a result of the fact that energy is transferred in the direction of decreasing temperature (Moran and Shapiro 2007).

C.1.2 Convection

Together with radiation, convection constitutes the two remaining thermal energy transfer methods. Convection represent energy transfer between a solid having an interface with either a moving gas, or a liquid. In a wax deposition regime, the flowing liquid will be the hotter medium, and the surface will act as the coolant. This gives the following relation for the thermal convection:

$$\dot{Q}_c = hA(T_{bf} - T_s) \tag{C.2}$$

Here the h represent the heat transfer coefficient, while A is the area and T_{bf} is the temperature of the hotter bulk fluid and T_s is the temperature of the pipe surface (Moran and Shapiro 2007). Both convection and conduction are controlling mechanisms to explain wax deposition.

C.1.3 Enthalpy

Since Fluent, the simulation software used in this report, bases its calculations on among other enthalpy and entropy these terms will be briefly explained here.

Enthalpy relates to the total energy in a thermodynamic system. It includes the internal energy, that ensures the energy required to establish a system, and the pressure and volume based energy term. Enthalpy is given by the expression below:

$$h = u + pv \tag{C.3}$$

The expression above is per unit mass, and u signifies the internal energy, while p is the pressure and v is the volume involved (Moran and Shapiro 2007).

C.1.4 Entropy

Entropy is a thermodynamic change in a reversible process, where the heat absorbed or emitted over the absolute temperature signifies this change. It is often referred to as the degree of unorder, and is defined as such:

$$dS = \int_1^2 \frac{\delta Q}{T} \tag{C.4}$$

where Q is the heat absorbed or emitted, T the temperature and S denotes the entropy (Moran and Shapiro 2007).

C.2 Thermal Analysis

For heat to be exchanged between two fluids, or a fluid and a solid, three specifications need to be present. First, the thermodynamic specifications that defines the

fluid flow in terms of the hot and cold fluid rates, and their inlet and exit temperatures. This relation is shown below:

$$Q = C_h(T_{h1} - T_{h2}) = C_c(T_{c2} - T_{c1}) \tag{C.5}$$

where C_h and C_c are the capacity rate for the hot and cold region respectively (Webb and Kim 2005).

Second, the rate of heat transfer between two regimes is dependent on the overall heat transfer coefficient between the two. Integrating equation C.5 with respect to the area provides the required heat exchanger area to satisfy the thermodynamic specifications involved. By doing this, in addition to presenting a relation for an effective mean temperature difference, one can state the heat transfer rate as follows:

$$Q = UA\Delta T_M \tag{C.6}$$

The mean temperature expression is a function of the heat exchanger flow geometry, such as cross flows or counter flows, and the degree of fluid mixing. The term UA is the overall thermal conductance, which is also the third specification that describes an heat transfer process (Webb and Kim 2005). By stating the expression $1/UA$ it gives the overall thermal resistance, which is the overall resistance to heat transfer between to regimes. The overall resistance is found by adding all the individual components resistance to heat transfer, shown in the expression below:

$$\frac{1}{UA} = \frac{1}{(\eta hA)_h} + (\frac{R_f}{A})_h + \frac{t}{k_w A_w} + \frac{1}{(\eta hA)_c} + (\frac{R_f}{A})_c \tag{C.7}$$

Here, the first and fourth term refers to the individual convective resistances belonging to the hot and cold regions respectively. The third term gives the conductive resistance, if a solid is separating the hot and cold regimes. The second and fifth term is the fouling resistances on the hot and cold surfaces if such effects exists

(Webb and Kim 2005). This expression is linked to thin walls, normally in transport of oil and gas thick walled pipes are used. So this is only presented to show the analysis.

Heat transfer is also affected by physical properties that change with temperature. If the region is very short, heat transfer may also vary with length due to entrance effects. For a wax deposition regime the occurrence of these effects are very likely. Properties such as viscosity and composition changes, in some cases drastically, in pipelines subjected to a temperature decrease. To account for these variations, one analogy is to look at the situation as a film temperature which is defined as an average of the local mixed fluid temperatures and wall temperature. An other analogy is to use the properties in the correlation that is evaluated at the mixed fluid temperature.

In literature the phenomenon of deposition falls within a group of mechanisms called fouling, and give rise to two of the terms in equation C.7. The deposits thermal resistance tends to reduce the overall heat transfer coefficient, and heat exchanger design is normally overcompensated when dealing with a fouling surface caused by deposition of material. The fouling factor can be seen as a combined expression of the resistance of a clean pipe, and a fouled one:

$$R_f = \frac{1}{U_{fouled}} - \frac{1}{U_{clean}} \tag{C.8}$$

Since the fouling of a surface is not constant with respect to time, the net fouling rate is described by the relation presented below:

$$\frac{dm_f}{dt} = \dot{m}_d - \dot{m}_r \tag{C.9}$$

This expression is identical to the deposition-release model, where the deposition rate is defined as the deposition rate minus the removal rate.

Webb and Kim (2005) defines three different categories of fouling, namely linear, asymptotic and a falling rate domain. The linear deposition occurs if the removal rate is insignificant, or if the deposition rate is constantly larger than the removal rate. An asymptotic scenario occurs if the deposition rate is constant throughout combined with a removal rate that becomes constant. The falling rate is found somewhat in between the two previously mentioned categories (Webb and Kim 2005). Different fouling mechanisms generally falls within different categories, where crystallization, chemical reaction, corrosion, and freezing fouling will behave as in the linear, or falling rate, regime. Particulate fouling is generally believed to show an asymptotic behavior.

The deposition mode is a function of the fouling mechanism, while the removal mode is dependent on the re-entrainmen rate, which is proportional to the shear rate at the surface (Webb and Kim 2005).

Webb et al. (2005) further presents a relationship for the deposition rate when being in a particulate fouling regime.

$$\dot{m}_d = SK_m(C_b - C_w) \tag{C.10}$$

where K_m is the mass transfer, C_b and C_w the bulk and wall concentration, respectively. However, in addition to these transport mechanisms, a sticking probability, S, has been incorporated into the deposition equation. The sticking probability is related to the presence of nucleation sites and the temperature regime in the area, and is a corrective factor.

As said previously, the removal rate is a function of the shear stress present at the surface.

$$\dot{m}_r = \frac{m_f \tau_w}{\xi} = \frac{\rho_f x_f \tau_w}{\xi} \tag{C.11}$$

The removal rate is described here as proportional to the shear stress, τ_w, fouling deposit thickness, x_f, and the fouling density, ρ_f and inversely proportional to a so called deposit bond strength, ξ (Webb and Kim 2005).

C.3 Heat Transfer in Wax Deposition

Paraffin wax exhibit an inherent low thermal conductivity, cited by among others Arasu et al. (Arasu et al. 2011). This results in an insulating effect as soon as a layer of wax has settled onto the pipe surface. It should therefore be possible, through an analysis of reduced heat transfer, to assess a deposited layer. Challenges in this will be linked to the characterization of the deposited layer, including aspects such as wax porosity, composition and roughness.

The deposited layer is not purely paraffin wax, but a mix of oil and a crystallized paraffin structure. The paraffin deposit will have a different heat conductivity than the entrapped oil, thus the layer's wax porosity need to be established before conducting any heat transfer modeling. As this porosity change with time, due to a process called "aging", the layer's thermal conductivity change accordingly.

The phenomenon of wax deposition is essentially a thermally driven process, which will not initiate before the temperature have dropped below the cloud point. However, after the wax particles have dissolved and formed crystals, other effects also controls the size and shape of the deposited layer. Such being, the degree of turbulence and composition of the mixture involved (Fong and Mehrotra 2007). This was shown in Fong and Mehrotra's text where the layer was found to be considerable thinner and harder for their turbulent experiments compared to samples subjected only to laminar flow made by Parthasarathi and Mehrotra (Parthasarathi and Mehrotra 2005). The deposition area is seen to decrease linearly as a function of the increase in logarithm of the Reynolds number. As the heat transfer is induced by an increase in Reynolds number, the convective thermal resistance is reduced in the bulk fluid. This also leads to a decrease in the deposits thermal resistance, ending in a thinner

deposit (Fong and Mehrotra 2007). The authors of the previous mentioned results illustrate this as the fact that the aging effect acts sooner and more speedy compared to laminar flow.

Singh et al. (2001) observed in their experiments that the deposit stops growing at a certain point in time, and that changes occurring after that is a result of aging. This was not found to change the thickness, but rather the composition and hardness of the deposited layer. As the deposit thickness grows, the insulating effect will increase accordingly leading to a decrease of further deposition (Singh et al. 2001). Thus, the size of the layer will depend on both the cooling rate and the compositions heat insulating ability.